Hair Cell Transduction, Tuning, and Synaptic Transmission in the Mammalian Cochlea

Robert Fettiplace[*1]

ABSTRACT

Sound pressure fluctuations striking the ear are conveyed to the cochlea, where they vibrate the basilar membrane on which sit hair cells, the mechanoreceptors of the inner ear. Recordings of hair cell electrical responses have shown that they transduce sound via submicrometer deflections of their hair bundles, which are arrays of interconnected stereocilia containing the mechanoelectrical transducer (MET) channels. MET channels are activated by tension in extracellular tip links bridging adjacent stereocilia, and they can respond within microseconds to nanometer displacements of the bundle, facilitated by multiple processes of Ca^{2+}-dependent adaptation. Studies of mouse mutants have produced much detail about the molecular organization of the stereocilia, the tip links and their attachment sites, and the MET channels localized to the lower end of each tip link. The mammalian cochlea contains two categories of hair cells. Inner hair cells relay acoustic information via multiple ribbon synapses that transmit rapidly without rundown. Outer hair cells are important for amplifying sound-evoked vibrations. The amplification mechanism primarily involves contractions of the outer hair cells, which are driven by changes in membrane potential and mediated by prestin, a motor protein in the outer hair cell lateral membrane. Different sound frequencies are separated along the cochlea, with each hair cell being tuned to a narrow frequency range; amplification sharpens the frequency resolution and augments sensitivity 100-fold around the cell's characteristic frequency. Genetic mutations and environmental factors such as acoustic overstimulation cause hearing loss through irreversible damage to the hair cells or degeneration of inner hair cell synapses. © 2017 American Physiological Society. *Compr Physiol* 7:1197-1227, 2017.

Didactic Synopsis

- Sound is detected by hair cells, the mechanoreceptors of the cochlea, the spiral cavity of the inner ear. Hair cells are excited by submicrometer vibrations of their stereociliary (hair) bundles, which are converted into changes in membrane potential graded with sound intensity.
- Hair bundles are bathed in an extracellular fluid, high in potassium and low in calcium and at a positive 100 mV potential, which optimizes the transduction process.
- There are two types of hair cell with disparate functions: outer hair cells contain prestin, a piezoelectric motor protein that generates force to amplify the mechanical stimulus, inner hair cells communicate with auditory nerve fibers via a ribbon synapse at the cochlear output.
- The frequency of a sound is analyzed by both passive and active tuning mechanisms, with subsets of hair cells along the cochlear being tuned to different frequencies.
- Transduction can be disrupted by mutations in single genes leading to permanent deafness; many of these genes are linked to the hair bundle structure.

Introduction

Since the last review in this series (56), which appeared nearly 30 years ago, knowledge of the mechanisms of transduction and transmission of auditory signals in the vertebrate cochlea has improved greatly. Progress has been driven by the use of isolated tissue preparations; the application of new techniques, such as patch clamping and cellular imaging; and the study of deafness mutants in both humans and mice. These developments have been reinforced at the clinical level by the employing otoacoustic emissions to assess electrical activity of the sensory cells and thereby diagnose hearing problems, especially in infants (3, 138). Moreover, treatment of sensorineural deafness has been transformed with cochlear implants to restore a degree of hearing by electrically stimulating the auditory nerve fibers in patients with hair cell loss or damage. The inventors of the electrical implants, Graeme Clark, Ingeborg Hochmair, and Blake Wilson, received the

[*]Correspondence to fettiplace@wisc.edu

[1]Department of Neuroscience, University of Wisconsin School of Medicine and Public Health, Madison, Wisconsin, USA

Published online, October 2017 (*comprehensivephysiology.com*)

DOI: 10.1002/cphy.c160049

2013 Lasker-DeBakey Medical Research Award (41, 42). All such advances drew on an established body of knowledge (144) initiated by the work of von Békésy (13), who described the cochlea as a spectrum analyzer that can separate different frequency components of a sound stimulus along its length. Low frequencies are at one end of the organ and high frequencies at the other, and the overall scheme is referred to as tonotopic organization. Pure tone stimuli (e.g., middle C on the piano at 260 Hz) evoke local vibrations of the basilar membrane. The motion due to these vibrations is detected by the sensory hair cells and transmitted synaptically to the dendritic terminals of auditory nerve fibers, resulting in precisely timed and synchronized firing in single fibers (144,255). Tonal stimuli of different frequencies generate spike discharges in different fibers, and the sound frequency is signaled to the brain according to which subset of fibers is active. Thus, the cochlea performs a Fourier analysis of the sound stimulus, and in the first stage of auditory processing, it can signal the amplitudes of disparate frequency constituents to the brain. This scheme raises several questions: (i) How do the hair cells detect the motion of cochlear membranes, particularly when the displacement amplitudes at threshold are of atomic dimensions? (ii) What types of receptor potential exist in the hair cells, and how are these potentials transmitted to the auditory nerve fibers? (iii) What mechanisms are recruited to discriminate between different sound frequencies and enable the narrow tuning needed for an accurate frequency analysis? The answers presented here will emphasize the importance of newer techniques, document ionic mechanisms unique to the cochlea that help to optimize auditory sensitivity, and assess lingering knowledge gaps. A recurring theme will be the clues furnished by gene mutations that have led to identification of the protein machinery underlying physiological functions. Neither cochlear development nor hair cell regeneration will be addressed, but recent reviews of both topics are available (10, 309). Much of the original hair cell research was performed on nonmammals such as frogs and turtles, but some significant functional differences exist between the vertebrate classes. Therefore, the observations and mechanisms delineated here will be based on information obtained from mammalian auditory preparations wherever possible.

The Hair Cell Environment

Structure of the cochlea

Sound pressure fluctuations are relayed to the cochlea in several steps. Vibrations of the eardrum are transmitted through three small middle-ear bones to generate pressure waves within the cochlea and to vibrate the basilar membrane (Fig. 1). This mechanical coupling ensures that sound energy is efficiently transferred from air to the cochlear fluids over a wide frequency range. Detection of the sound stimulus and its conversion to an equivalent electrical waveform, termed mechanoelectrical transduction, occurs in the sensory hair cells riding on the basilar membrane. The mammalian cochlea contains two hair cell classes, inner and outer, and each has distinct functions. Information about the acoustic environment is conveyed to the auditory nerve fibers almost exclusively via the electrical signals of inner hair cells (IHCs), whereas the main task of outer hair cells (OHCs) is to boost the stimulus by mechanically amplifying the sound-driven vibrations of the cochlear partition.

Before considering the transduction mechanism, it is instructive to describe the compartments of the inner ear and their ionic distributions, which are relevant for hair cell

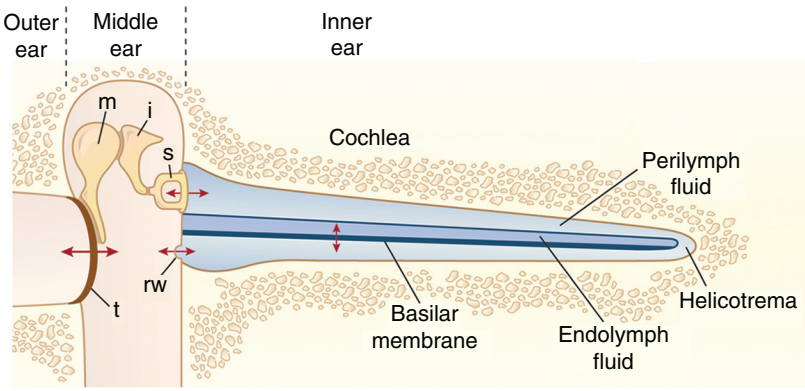

Figure 1 Schematic of the sound transmission pathway from the eardrum to the cochlea. Sound stimuli impinge on the tympanum (**t**), or eardrum, at the end of the ear canal and the vibrations (denoted by red arrows) are transmitted through the three bones of the middle ear: malleus (**m**), incus (**i**), and stapes (**s**). The footplate of the stapes behaves like a piston in the oval window and initiates pressure waves in the cochlear fluids so setting in vibration the basilar membrane. The pressure is relieved at the round window (**rw**). The cochlea, here depicted as straight, is *in situ* coiled like a snail's shell and embedded in the petrous temporal bone. It is subdivided into three compartments containing perilymph or endolymph fluid, the two outer compartment being connected by the helicotrema. The total length of the cochlea is 35 mm (humans), 26 mm (cat), 18 mm (guinea pig), and 6 mm (mice).

transduction. Each cochlea is a fluid-filled tube roughly 0.2 mm in diameter the length of which varies by species from ~6 mm in mice to 35 mm in humans. The cochlea is coiled like a snail's shell so it can be housed compactly in the temporal bone at the base of the skull. The number of turns differs somewhat among species from about two and a half in mice or humans to four in guinea pigs or chinchillas. The cochlea is in fluid continuity with other parts of the inner ear, including the saccule, utricle, and three semicircular canals, which compose the vestibular labyrinth. The cochlear duct is partitioned into three compartments: two outer scalae (tympani and vestibuli) and the scala media. The outer scalae are interconnected via the helicotrema at the cochlear apex and envelope the scala media (Fig. 1). The scala media is delimited by aforementioned Reissner's membrane, the spiral ligament laterally and the basilar membrane below (Fig. 2). Surmounting the basilar membrane is the organ of Corti, a structurally complex epithelium that includes four rows of hair cells shrouded by six or more types of uniquely shaped supporting cells with distinct names (e.g., Hensen's cells and Deiters' cells). Among other functions, these cells endow the assembly with strength and deformability as it vibrates in response to sound.

Endolymphatic fluid compartment

The supporting cells of the organ of Corti and their junctional complexes with the hair cells collectively function as a tight epithelium to isolate the fluid of the scala media, the endolymph, from that of the scala tympani, the perilymph (Fig. 2). On the surface of the organ of Corti, three rows of OHCs intercalate with apical phalangeal processes of the Deiters cells and are separated from the IHCs by the top surfaces of the pillar cells. Since the ionic compositions of

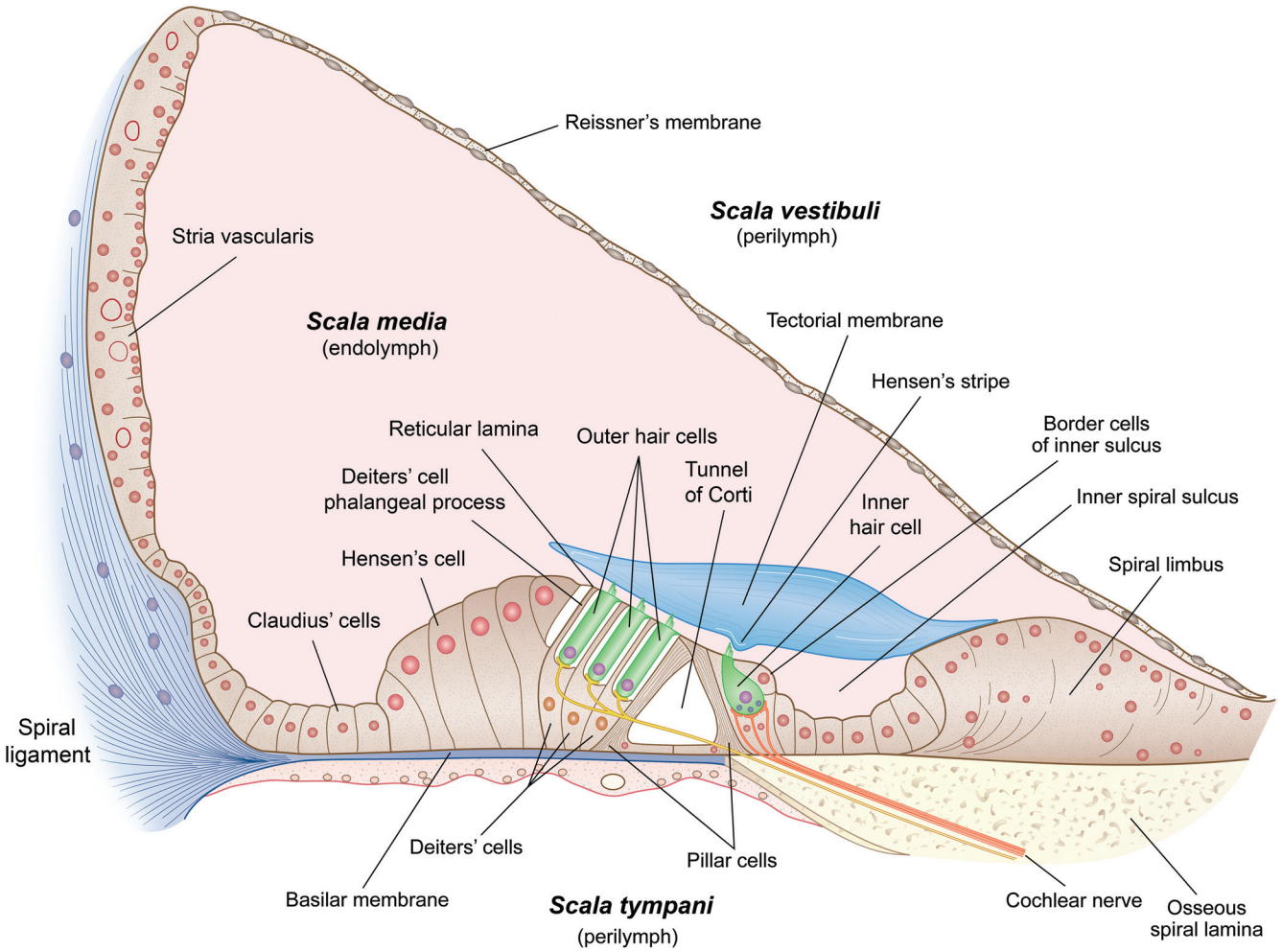

Figure 2 Cross section though the cochlear duct showing the cellular structure. The scala media is delimited by Reissner's membrane, the spiral ligament, and the basilar membrane, which is surmounted by the organ of Corti. The width of the basilar membrane ranges from approximately 100 to 500 μm in humans. The scala media is filled with a K^+-based endolymph, here colored pink. The organ of Corti contains the sensory hair cells embedded in assorted supporting cells of distinct shape. The hair-cell stereociliary bundles are covered in an acellular tectorial sheet and the cells are innervated by the cochlear branch of the VIIIth cranial nerve. Inner hair cells are contacted by afferents (orange) whereas outer hair cells are innervated mainly by efferent fibers (yellow). The stria vascularis is an epithelial strip on the lateral wall that is specialized for secreting endolymph.

the fluids above and below the organ of Corti are quite different, complete isolation across the epithelium is essential. This isolation is maintained by claudin-based tight junctions between the cells (15). The scalae tympani and vestibuli contain perilymph that is virtually identical to plasma or cerebrospinal fluid, but the scala media is filled with endolymph, which resembles intracellular fluid, with K^+ as the predominant cation and low amounts of Na^+ and Ca^{2+}. In mammals, the typical ionic concentrations (in mmol/L) of perilymph are 148 Na^+, 4 K^+, 1.3 Ca^{2+}, 1 Mg^{2+}, 119 Cl^-, and 21 HCO_3^-, pH 7.4; in endolymph, the concentrations are 1 Na^+, 157 K^+, 0.02 Ca^{2+}, 0.01 Mg^{2+}, 132 Cl^-, and 30 HCO_3^- (297). In addition, a large voltage difference, the endolymphatic potential (EP), exists between the two compartments, with the scala media being about 80 to 100 mV positive to the scala tympani [rats (28); guinea pigs (27, 96); mice (279); cats (276)]. In animal experiments, the positive EP was decreased, often to a negative value, by anoxia or application of loop diuretics such as furosemide or ethacrynic acid that interfere with Na-K-Cl cotransporters (27, 28, 31, 276). The large EP is thought to be due to active K^+ transport into the endolymph; reduction of the potential to −40 mV during anoxia suggests a passive diffusion potential dependent upon the K^+ gradients between endolymph and perilymph (27). Thus, during lack of oxygen, the active component of the EP is lost, and what remains largely reflects the Nernst potential of the K^+ concentration gradient between endolymph and perilymph. As discussed later, the composition of endolymph and the magnitude of the EP are crucial for optimizing hair cell transduction. For example, a decrease in EP, induced either by hypoxia or loop diuretics, reduces both the sensitivity and frequency selectivity of the hair cell and auditory nerve fiber tuning curves (31, 74). It also greatly reduces the sound-induced vibrations of the basilar membrane (259).

Endolymph secretion and the stria vascularis

The unusual composition of endolymph and the EP are produced during fluid secretion by the stria vascularis, a specialized epithelial segment of the spiral ligament located on the side wall of the cochlear duct [Fig. 3; (297)]. The stria vascularis has two main cellular layers, the marginal cells facing the endolymph and the basal/intermediate cells, which are interconnected by gap junctions and exposed to perilymph. In each layer, adjacent cells are linked by tight junctions. If these tight junctions are disrupted on the basal cell epithelium by knocking out claudin11, a constituent of the tight junctions, the EP is degraded without an immediate drop in the high K^+ concentration in endolymph (104, 147). This observation suggests the two properties are distinct. This notion is consistent with the arrangement in nonmammals (such as the chicken), in which the endolymphatic duct has high K^+ but a small EP (<20 mV). Evidence on the origin of the EP was derived from experiments in which a voltage electrode was inserted through the strial epithelium to map potential gradients across the cell layers (212, 266). This approach revealed that an intrastrial

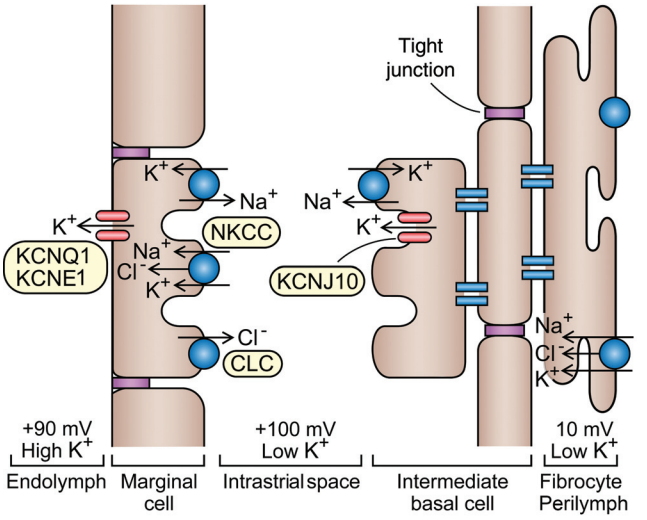

Figure 3 Schematic of the stria vascularis. The stria comprises two cellular layers separated by an intrastrial space. Marginal cells face the endolymph and intermediate/basal cells, interconnected by gap junctions (blue pairs of lines), are exposed to fibrocytes of the strial ligament and perilymph; adjacent cells in each layer are linked by tight junctions (purple). (Note that the orientation is reversed with regard to that shown in Fig. 2.) Flow of K^+ ions is facilitated by the inwardly rectifying KCNJ10 K^+ channel on intermediate cells and the KCNQ1/KCNE1 K^+ channel on the endolymphatic aspect of the marginal cells. Ionic balance is maintained by Na/K ATPase, Na-2Cl-K and Cl transporters. The voltages given (+90, +100, and +10 mV) refer to the static potentials of the extracellular spaces with respect to the scala tympani. The endolymphatic potential of +90 mV is attributable to a Nernst K^+ equilibrium potential of ~100 mV across the highly K^+ selective apical membrane of intermediate cells. The intrastrial space has low K^+ due to uptake of the ion by the Na-2Cl-K cotransporter and the Na/K ATPase and K^+ is then secreted into endolymph across the K^+-selective membrane of marginal cell.

fluid layer with very low K^+ concentration is sandwiched between the two cellular sheets, but it sits at a large positive potential similar to the EP. The EP is therefore not generated by the outermost marginal cells but appears to depend on the K^+ equilibrium potential across the apical membranes of intermediate cells (Fig. 3). The intermediate cells are electrically coupled through gap junctions formed by connexin-26 and connexin-30 (172) to the basal cells and to fibrocytes in the spiral ligament, all of which have an unusually low resting potential of about −5 mV. In contrast, the cytoplasmic K^+ concentration is high in both intermediate and marginal cells but is low in the extracellular intrastrial space between them. If the K^+ concentration was 3 mmol/L in the intrastrial space and 157 mmol/L in the cytoplasm of the intermediate cells, the K^+ equilibrium potential would be −105 mV; with an intermediate cell resting potential of −5 mV, the intrastrial space is estimated at +100 mV. Thus, the current hypothesis is that the EP is largely attributable to a Nernst K^+ equilibrium potential of ~100 mV across the apical membrane of the intermediate cells, which are rendered highly K^+ selective because of the presence of inwardly rectifying K^+ channels (Kir4.1, encoded by the *KCNJ10* gene). Consistent with this notion, knock-out of *KCNJ10* abolishes the EP (189). K^+

from the intrastrial space is taken up into the marginal cells by a Na-2Cl-K cotransporter (64, 83) and a Na/K ATPase, and it is secreted into endolymph (300) across the apical membrane of the marginal cell; the latter membrane is also very selective for K^+ due to the K^+ channel composed of KCNQ1 and KCNE1 subunits (126, 210, 297).

Mutations of ion channels and transporters in the stria vascularis

Mutations in any of the ion channel/transporter genes, including *KCNJ10*, NaK2Cl (*NKCC1*), and *KCNQ1*, result in loss of EP and deafness, but other genes can play a part in the process and their mutations also affect the EP. One example is the gene *SLC24A4*, which encodes the protein pendrin (75), an anion (Cl/HCO_3) exchanger in the epithelial cells that pumps HCO_3^- into the endolymph. The primary consequence of an *SLC24A4* mutation is acidification and enlargement of the endolymphatic system (298), but secondary consequences include loss of KCNJ10-containing channels and the EP in the Pendred syndrome mouse (299, 301). Another example is the gene *GJB2*, which encodes the gap-junction protein connexin-26. Mutations of this protein are associated with the most common form of autosomal nonsyndromic hearing loss. Connexin-26 forms hemi-channels at the cell surface and gap junctions between cells, and it occurs in many cells of the spiral ligament, including between the cells of the stria vascularis. The exact mechanism of the hearing loss remains controversial (298, 306); however, deletion of connexin-26 expression in the cochlea causes over 50 percent reduction in EP as well as a decrease in endolymphatic K^+ concentration (43). Mutations in the genes encoding pendrin and connexin-26 are responsible for more than 50% of all cases of prelingual sensorineural deafness in the Caucasian population.

Endolymph calcium

A second critical feature of endolymph is its unusual Ca^{2+} concentration. This concentration has been measured by several groups through direct fluid sampling or use of double-barreled Ca^{2+}-selective electrodes, yielding values between 20 and 40 μmol/L in rats (28), guinea pigs (96, 123, 265), and mice (308), much lower than the 1.3 mmol/L in perilymph. The Ca^{2+} concentration in endolymph was found to abruptly increase with anoxia or administration of loop diuretics (28, 123). To address how this low Ca^{2+} concentration is achieved, the endolymphatic compartment may be considered as a cell with a resting potential of +90 mV. As with the K^+ ion, endolymph Ca^{2+} is not in equilibrium: for an EP of +90 mV and a perilymphatic concentration of 1.3 mmol/L, the Ca^{2+} concentration in endolymph predicted from the Nernst equation should be ~1 μmol/L. It being 20-fold higher implies active transport of the divalent ion into the endolymph. One of the main site of pumps for actively transporting Ca^{2+} is on the hair cell stereocilia, where they extrude Ca^{2+} that has accumulated cytoplasmically because of influx through the hair cell mechano-electrical transducer (MET) channels or voltage-sensitive Ca^{2+} channels. Ca^{2+} pumping is a crucial feature of cochlear hair cells (20), and it is implemented via a plasma membrane Ca^{2+} ATPase (289, 313) as the PMCA2a isoform (68). The importance of the hair cell PMCA2 pumps is emphasized by their high density (>2000/μm^2) in OHC stereocilia (39). Their sustained operation is a considerable drain on the hair cells' energy supply. As might be expected, several PMCA2 mutations are linked to deafness (150, 179, 278, 280). In one such deaf mutant, the deafwaddler *dfw2J* mouse, the truncated PMCA2 is totally absent from the stereocilia, and the endolymphatic concentration is consequently reduced from 23 μmol/L to a near passive value of 6.6 μmol/L (308). In another mutant (278), the defective PMCA2 is still present in the stereocilia, but its pumping activity is diminished and is therefore unable to clear the Ca^{2+} load. As a consequence, the mouse displays progressive hearing loss, beginning at the base of the cochlea in high-frequency OHCs, which might be expected to be the most susceptible to Ca^{2+} overload (20). The multiple roles of Ca^{2+} in hair cell function will be described in a later section, but it should be noted here that reducing the Ca^{2+} in the endolymph bathing the hair cell stereociliary bundles to a low micromolar concentration will abolish mechanotransduction (9, 52).

In summary, the sensory hair cells are situated in a tight epithelium within the organ of Corti. Their transducing apparatus, the hair bundles, project apically into endolymph rich in K^+ and containing a critical 20 μmol/L concentration of Ca^{2+}. In contrast, the basolateral surface of the hair cells, where the auditory nerve terminals synapse, is exposed to perilymph, which normally has 1.3 mmol/L extracellular Ca^{2+} to support synaptic transmission and high Na^+ for action potential generation. Transduction, the main aspect of hair cell function, will now be considered.

Hair Cell Transduction

The hair bundle

Transduction, the conversion of sound to an equivalent electrical waveform, occurs in the mechanoreceptive hair cells anchored in the organ of Corti. The proximate mechanical stimulus is deflection of the hair bundles against the overlying acellular tectorial membrane. Sound-driven deflections of the basilar membrane are translated into approximately equal radial displacements of the hair bundles, culminating in activation of MET ion channels in the bundle. The hair bundle is a complex and tightly regulated organelle (12) that comprises 50 to 100 microvilli, termed stereocilia. Each stereocilium is about 200 nm in diameter in OHCs and twice that in IHCs. The stereocilia are reinforced along their length by a paracrystalline array of parallel actin filaments (both β- and γ-isoforms) that are cross-linked with several actin-binding proteins, including espin, the mutation or knockout of which causes severe hearing loss (321). OHC stereocilia are arranged in three V-shaped rows, with their distal tips inserted into

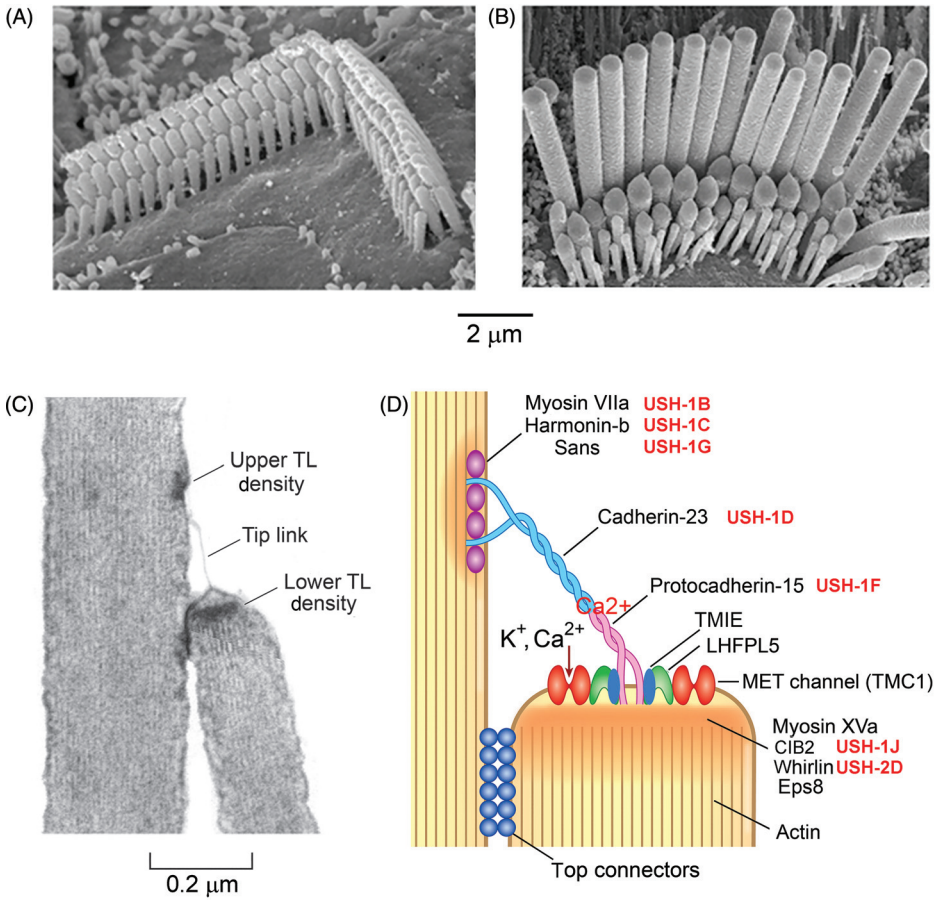

Figure 4 Stereociliary bundles and the transduction apparatus. Scanning electron micrographs of stereociliary bundles of (A) an outer hair cell and (B) an inner hair cell, showing the staircase in heights of the rows. (C) Transmission electron micrograph of an outer hair cell showing a tip link connecting two stereocilia; the insertion sites of the tip link (TL) are heavily electron dense suggesting dense protein densities. (D) Schematic of the molecular structure of the tip link apparatus deduced from various mutations. USH-1 and USH-2 denote different Usher type 1 and type 2 mutations. The association between the N-termini of protocadherin-15 and cadherin-23 is Ca^{2+} dependent. Two MET channels (red) are situated at the lower end of the tip link and are present as complexes with TMIE, LHFPL5, TMC1, and possibly other proteins. Modified, with permission, from (80).

pockets on the underside of the tectorial membrane (4, 170). Such attachment may serve as a tight mechanical coupling between the two structures, but the functional significance of the V-shaped organization is unknown. Multiple rows of stereocilia are arranged in a staircase pattern that increases in height from one edge to the other (Fig. 4); the shape and dimensions of the bundle vary with position along the cochlea, with more numerous and shorter stereocilia in progressing from the apex to the base of the cochlea (170, 256).

The stereociliary staircase is associated with a functional polarization such that (positive) deflections of the bundle toward its taller edge are excitatory and cause MET channels to open, whereas (negative) deflections toward its shorter edge cause MET channels to close (80). All hair bundles are oriented in precisely the same abneural direction to confer a common response polarity during basilar membrane motion. When deflected, the component stereocilia move in synchrony, pivoting at their tapered basal insertion (51, 151) into the cuticular plate, an amorphous actin network beneath the apical plasma membrane (234). At the tapered ankle of each stereocilium, there are fewer actin filaments cross-linked with another actin-bundling protein, TRIOBP (148). To provide both structural and functional cohesion to the bundle, the component stereocilia are interconnected by various extracellular filaments that are identified according to the distance above the top of the cell and their molecular composition; these filaments include ankle links, lateral links, top connectors, and most importantly tip links. In rodent cochlear hair cells, the ankle links and lateral links are transient and disappear by the onset of hearing at postnatal day (P) 12 in mice (100, 231), at which time the top connectors associated with the protein stereocilium develop (291). The tip links, extending from the tip of one stereocilium to the side wall of its taller neighbor, are essential for applying force to the MET channels, and their destruction totally eliminates transduction (9, 91). Since the tip links run parallel to the bundle's plane

of symmetry, they are all stretched by positive deflections of the bundle and relaxed by negative deflections, so accounting for the functional polarization (91,232). The interciliary coupling ensures that a bundle's MET channels are coherently activated to maximize sensitivity. The channels are thought to be confined to the tops of the second and third row stereocilia at the lower end of the tip link (17). When Ca^{2+} influx through the MET channels was imaged in IHCs and OHCs on a millisecond time scale with a fluorescent dye, the tallest row of stereocilia had a negligible signal compared with the other two rows, implying that the upper end of the tip link has no channels.

Mechanoelectrical transducer currents

The electrical events in the hair cell resulting from hair bundle stimulation have been extensively documented from hair cell recordings in both nonmammals [frog (9, 116); turtle (51); and chicken (284)] and in mammals (16, 94, 112, 127, 140, 155). Hair cells in altricial rodents such as rats, mice, and gerbils have been mainly investigated in the first 2 weeks after birth, when the bony shell of the cochlea is easier to open without causing mechanical trauma to the hair cells. The delicate process of opening the cochlea becomes increasingly difficult with age and ossification. However, circumstantial arguments, bolstered by a few direct measurements, suggest the number and properties of the MET channels are mature by P12 at the onset of hearing in these rodents (112,129,140). In all these cases, experiments were performed on hair cells in segments isolated from different regions of the cochlear spiral. Positive step displacements of the tip of the bundle evoke an inward MET current at the negative resting potential, with a rapid onset of the current to a peak graded with the size of the step [Fig. 5; (140,247)]. Usually, a fraction of the channels are open at rest, so negative deflections close those channels. The detailed functional properties of the MET channel have been amply reviewed (80,81,120,229) and will only be summarized here with an overview of ionic selectivity, response kinetics, and molecular structure.

Transducer channel ionic selectivity and block

The MET channels are permeable to all small cations, with the permeabilities to Na^+ and K^+ being approximately equal and each of those permeabilities being a quarter of that to Ca^{2+} (16,216). Owing to the composition of endolymph, K^+ carries most of the inward MET current to generate a depolarizing receptor potential. During channel opening, K^+ flows across the apical stereociliary membrane of the hair cell, down a voltage gradient consisting of the resting potential [−40 to −60 mV; (112, 129)] and the EP (100 mV), which together give a total electrical gradient of ∼150 mV to augment the current. K^+ ions leave the hair cell across the basolateral membrane and down a concentration gradient into low K+ perilymph; the cell thus expends no energy in maintaining the ionic gradient, and the requirement for ATP consumption is transferred to the stria vascularis to fuel the secretion of endolymph. This unusual arrangement is especially beneficial to small hair cells with a large area-to-volume ratio whose cytoplasmic ion concentrations could otherwise change substantially during extensive activity. The composition of perilymph facing the basolateral aspect of IHCs, with high Na^+ concentration and Ca^{2+} similar to extracellular fluid, is also necessary because it enables the synapse to be regulated in the usual Ca^{2+}-dependent fashion and Na^+-dependent action potentials to be generated in the auditory nerve.

The MET channel is a large ion channel that discriminates poorly among cations. It is also significantly permeable to bulky organic ions, which has allowed estimating the pore size as being over 1.2 nm (76). Examples of large permeable organic cations include tetraethylammonium, which has about a quarter the permeability of K^+ (76,216), and molecules such as the styryl dye FM1-43, which has a molecular weight of 611 (92), and the antibiotic dihydrostreptomycin, which has a molecular weight of 584 (188). The latter two agents block the MET channel but also traverse it; they are permeant blockers, an attribute that has important implications. Lighting up the hair cell with the fluorescent dye FM1-43, which can enter and insert into intracellular membranes, has become a routine method of assaying for functional MET channels. This method can be used to test for channel mutants (135, 197). In contrast, the permeability to dihydrostreptomycin and its congeners is clinically significant because cytoplasmic access of these aminoglycoside antibiotics and their targeting to the mitochondria likely underlie their ototoxicity (122,295). One other manifestation of the MET channel size is the unexpectedly large single-channel conductance of 100 pS or more, which may be contrasted with 30 pS for a common cation channel like the acetylcholine receptor [Fig. 12.8 in reference (114)]. Single MET channels have been measured using whole-cell recording after severing the majority of the tip links by exposure to submicromolar Ca^{2+} (16, 52, 244). Such a low Ca^{2+} concentration is achieved by adding calcium-chelating agents like BAPTA, and it is reasoned that this treatment destroys almost all tip links and closes attached MET channels, leaving one or two channels that can be characterized with whole-cell recording. Justification of the technique is supported by the observation that similar values for unitary conductance can be measured under other conditions not necessitating exposure to BAPTA (23, 94, 216). Another unanticipated conclusion from measuring single MET channels is that their conductance changes, increasing by up to three fold in progressing from the cochlear apex to the base [Fig. 6; (16,244)]. The macroscopic MET current increases in amplitude along the cochlea, generated by variations in both unitary conductance and numbers of stereocilia per bundle [Fig. 5; (16)]. The function of such a gradient is most likely to enhance auditory sensitivity in high-frequency hair cells at the base where the basilar membrane is the most rigid.

The MET channel is blocked by various polyvalent cations, ranging from ions such as Gd^{2+}, La^{3+}, and ruthenium red to organic molecules like FM1-43, dihydrostreptomycin, benzamil, and curare, all with half-blocking concentrations

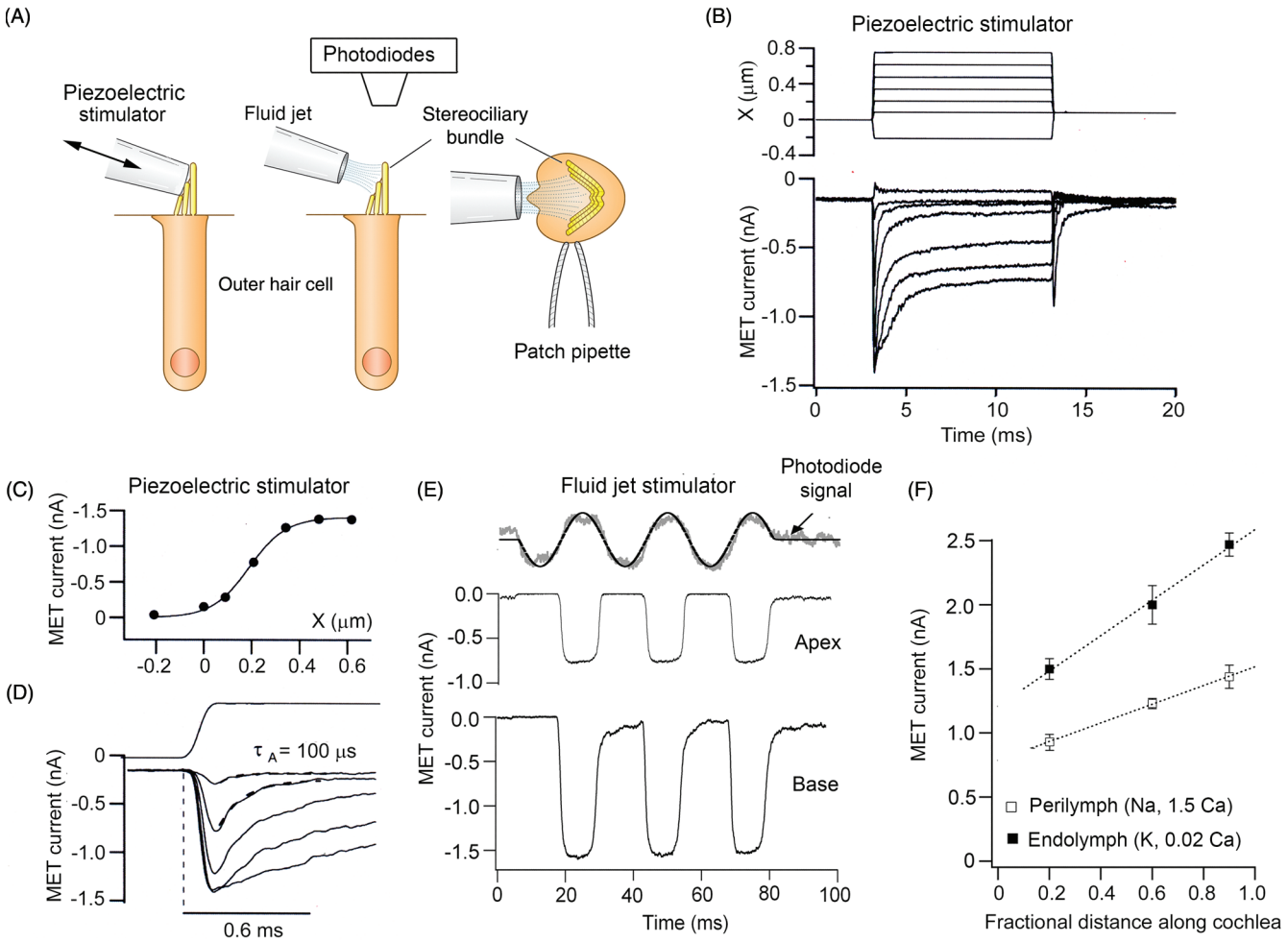

Figure 5 Mechanoelectrical transducer (MET) currents in outer hair cells. (A) Schematic of the stimulating and recording techniques. OHCs are patch clamped and the stereociliary bundle is deflected either by a glass probe attached to a piezoelectric device or by a fluid jet. Displacement of the bundle are calibrated by projection of image onto a photodiode array (55, 243). (B) MET currents for family of step displacements, X, of a hair bundle, displaying rapid rise to peak and then adaptive decline to a steady level. (C) Plot of peak MET current against bundle displacement with an operating range of ~0.25 μm. (D) Expanded scale of MET current onset showing that it develops as quickly as the displacement step (shown above) but then adapts with a time constant, τ_A, of 100 μs. (E) MET currents in OHCs from the apex and base of the cochlea for sinusoidal modulation of hair bundle position (top). Bundle motion was calibrated by projecting its image on to a pair of photodiodes, the noisy grey trace denoting the photocurrent. (F) MET current increases from apex to base of cochlea; current amplitude was 50% larger in the reduced Ca^{2+} of the endolymph solution-bathing bundle. All currents measured at a holding potential of −84 mV. Modified, with permission, from (80, 146).

on the order of 1 to 10 μmol/L [reviewed in (80)]. No agent with very high affinity is known. The most active, which has a half-blocking concentration of 0.6 μmol/L, is the 34-residue spider toxin GsMTx-4 (19), which also blocks other mechanosensitive ion channels (11, 282). The blocker with the most physiological significance is Ca^{2+}, and although its affinity is low, its half-blocking concentration of 1 mmol/L is in the range of Ca^{2+} concentration in plasma. Therefore, lowering the Ca^{2+} concentration from 1.3 mmol/L of perilymph to the 0.02 mmol/L in endolymph fully relieves the block and boosts the amplitude of the single-channel and macroscopic MET currents by about 50% (244). However, further reduction in the endolymph Ca^{2+} concentration is unacceptable because it destroys the tip links. The precise Ca^{2+} concentration at which this occurs is not known for certain, but it is probably about 5 to 10 μmol/L; in the *deafwaddler PMCA2a* mutant, the MET current is lost at an endolymph Ca^{2+} concentration of 6 μmol/L (308). As discussed later, Ca^{2+} contributes to the structural integrity of the tip link by stabilizing the interaction between two of its components, cadherin-23 and protocadherin-15. Besides blocking the MET channel and supporting the integrity of the tip link, Ca^{2+} plays a third role in triggering intracellular processes following its entry into the stereocilia via the MET channel, namely, adaptation of the MET current (8, 47, 51, 70, 80, 245).

Transducer channel activation and adaptation

Operating range

Displacements of the hair bundle are proposed to exert force on the MET channel by extending a "gating spring" in series with the channel (119), similar to the way in which force

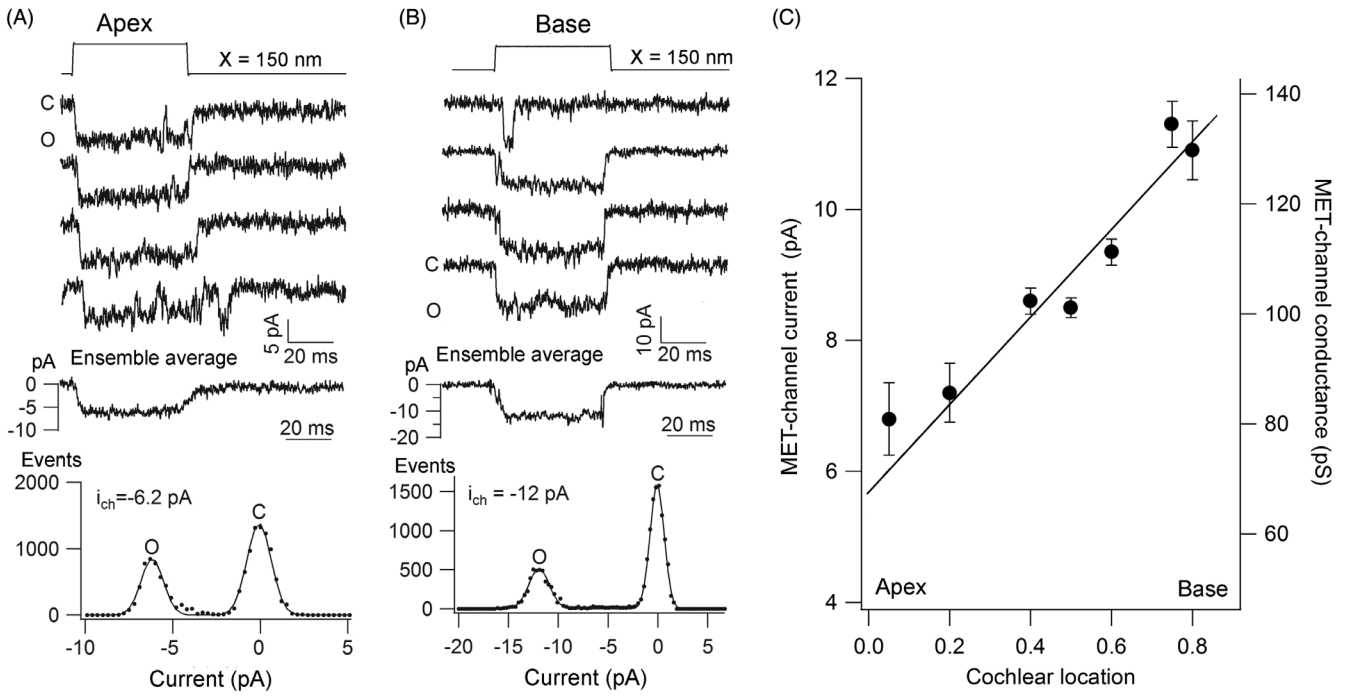

Figure 6 Single MET channels in mouse hair cells. (A) Apical outer hair cell: four representative single channel records for 150 nm hair bundle displacement steps; middle, ensemble average of 10 responses; bottom amplitude histograms giving mean single-channel current of 6.2 pA. (B) Basal outer hair cell: four representative single channel records for 150 nm hair bundle stimuli; middle, ensemble average of 10 responses; bottom, amplitude histograms giving mean single-channel current of 12 pA. (C) Single-channel current and conductance (mean ± 1 SD) as a function of position in the cochlea, expressed as relative distance from the apical end. Total length of cochlea is 6 mm. All measurements made at room temperature and −84 mV holding potential. Modified, with permission, from (23).

can be applied by stretching a macroscopic spring. The MET current is graded with bundle deflections up to ~100 nm, and the relationship between the peak current and displacement, X, can be described by a Boltzmann equation. A single Boltzmann fit is expected for a two-state channel in which mechanical energy modulates the transition between a closed state and an open state. Using this scheme, the open probability of the channel, p_O, can be specified as

$$p_O = 1/\{1 + \exp[Z(X_O - X)/k_BT]\} \quad (1)$$

where X_O is the displacement to half activate the current, Z is the single-channel gating force (a measure of the sensitivity of transduction), k_B is Boltzmann's constant, and T is absolute temperature. Z can be related to Λ, the range of hair bundle displacements (190) over which the open probability of the channel changes from 10% to 90%:

$$\Lambda = 4.4 \cdot k_BT/Z \quad (2)$$

Compared to other mechanoreceptors, such as those in the skin, hair cell transduction is exquisitely sensitive and responds maximally over a tenth of a micrometer, 100-fold less than cutaneous mechanoreceptors. The working range, estimated from the value of Λ, depends on the method employed for deflecting the bundle (80, 206), but best estimates are 50 to 100 nm for OHCs in mouse, rat, or gerbil cochleas. In an isolated hemi-cochlea preparation under more physiological conditions (112), stimuli were delivered to the basilar membrane, and the values for Λ calculated from hair cell recordings ranged from 50 nm for basal OHCs to 190 nm for apical OHCs. These bundle displacements are comparable to the vibration amplitudes of the basilar membrane measured in intact animals. The latter amplitudes can be inferred from the range of movements over which the nonlinearity between sound pressure and basilar membrane displacement is observed. As discussed in the section on cochlear frequency tuning, the nonlinearity arises from contractions of the OHC body driven by receptor potentials generated by forward transduction, and it will only be apparent for stimuli that modulate the opening of the MET channels. Therefore, vibrations of the basilar membrane are only amplified by OHC motility for stimuli over which the open probability of the MET channels varies, from rest to maximum. Several complete measurements of basilar membrane motion are available, and most displacement amplitudes interpolated from the upper extent of the nonlinearity fall within a span of 30 to 100 nm (220, 242, 254, 260). It is suggested that these displacement limits signify the operating range of the MET channels.

Activation kinetics

MET currents evoked by step displacement of the bundle display a rapid onset to the peak and then decline in several phases of adaptation (Fig. 5). While the submillisecond activation kinetics have been determined for MET currents in frog

and turtle hair cells (47, 51, 247), measuring the much faster activation kinetics of MET currents of mammalian cochlear hair cells has so far proved impossible. For these cells, the time course for hair bundle displacement is rate limiting because the stimulus rise time cannot be reduced below ~50 μs with the use of conventional piezoelectric stimulators (247). Furthermore, the bandwidth of whole-cell patch-clamp recording may also be limiting, so even if the stimulus was fast, the MET current could not be faithfully recorded. The activation kinetics of the channel must be sufficiently fast so as not to filter the MET current for high-frequency sinusoidal stimuli. One piece of evidence in support of this notion is that (sinusoidal) cochlear microphonics (thought to be dominated by the OHC transducer current) can be recorded at more than 60 kHz in mammals with high-frequency hearing, such as bats (261). In mice, if hair cells faithfully transduce frequencies as high as the upper frequency limit, then for animals that possess auditory nerve fibers tuned to at least 70 kHz (283), the limiting time constant is $1/\{[2\pi(7 \times 10^4]\}$ s ≈ 2 μs. With present techniques, a current rise time of this speed is unresolvable and will appear to be contemporaneous with the stimulus. However, a new solid-state nanoscale cantilever has recently been developed that can produce step deflections in less than 10 μs (65). Provided the recording bandwidth can also be expanded, this stimulation technique may improve the measurements to the point that the kinetics of cochlear hair cell MET channels may be directly quantifiable. This outcome will be an important accomplishment because it will provide a quantitative measure of the limiting rate at which an ion channel can activate.

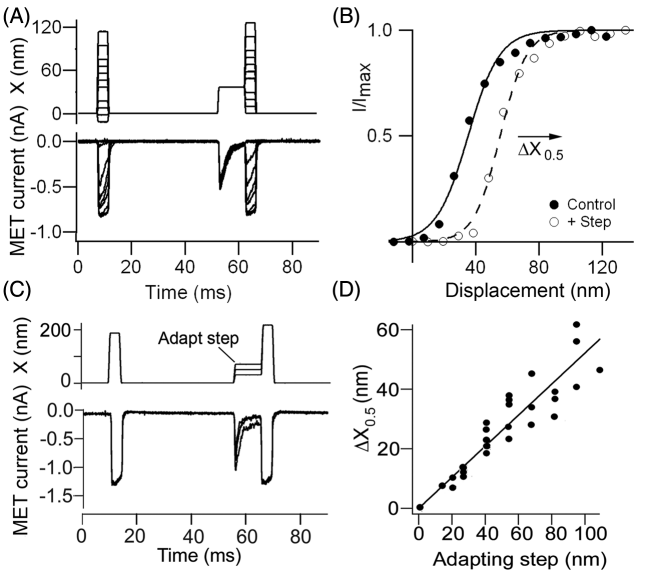

Figure 7 Adaptation assayed with two-pulse experiment. (A) MET currents for two series of brief bundle displacements, the first are control steps and the second are test steps, which are preceded by a long adapting step. Note the current decay during the adapting step. (B) Current-displacement relationships for first (control) pulse and for second (test) pulse after adapting step. The current I is scaled to its maximum value, I_{max}. Note the positive shift, $\Delta X_{0.5}$, in the current-displacement relationship. (C) Schematic of experiment where the amplitude of the adapting step was varied. (D) Plot of shift in current-displacement relation, $\Delta X_{0.5}$, as a function of the size of the adapting step. The slope is typically 0.5–0.6. All currents measured in outer hair cells at a holding potential of −84 mV. Results, with permission, from reference (18).

Transducer adaptation and Ca^{2+}

MET currents are also shaped by adaptation. As in other sensory receptors, the role of this adaptation is to offset responses to sustained stimuli, thereby preventing saturation of the current and optimizing sensitivity by maintaining the MET channels within a narrow operating range. This process is astonishing because it necessitates adjusting the mechanical input to the MET channel to a few nanometers; the diameter of the stereocilium is only 200 nm. Two major processes with different time frames are commonly recognized: fast adaptation, which operates on a millisecond or sub-millisecond time scale, and slow adaptation, which acts over tens of milliseconds (8, 51, 69, 70, 294, 311). The exact mechanisms underlying either form of adaptation are still controversial, but both are thought to be regulated by intracellular Ca^{2+}, at least in nonmammals. Evidence supporting this notion in frog and turtle hair cells includes the following: (i) the fast adaptation time constant is slowed by lowering the extracellular Ca^{2+} concentration (245, 248); (ii) adaptation is abolished by depolarizing the cell to +80 mV, thereby preventing Ca^{2+} influx (8, 52); and (iii) the position of the current-displacement (I-X) relationship on the displacement axis is sensitive to the extracellular Ca^{2+} concentration and the intracellular Ca^{2+} buffering (111, 248). The current hypothesis is that changes in the Ca^{2+} concentration within the stereocilia reset the range of bundle displacements over which the MET channel is activated. The shift may be assayed by using a brief test pulse either alone or superimposed on an adapting step (Fig. 7). Increased Ca^{2+} influx, as occurs during a prolonged excitatory step, shifts the I-X relationship positive to larger displacements, with the extent of the shift being proportional to the adapting step. Reducing Ca^{2+} influx, by either channel closure or a decrease in the extracellular Ca^{2+} concentration, shifts the I-X relationship in the opposite direction. An implication of the latter property is that the channel's resting open probability, p_{OR}, depends on extracellular Ca^{2+} concentration; under physiological conditions, where the bundles are exposed to a 0.02 mmol/L Ca^{2+} concentration of endolymph, about half the MET channels in OHCs are open at rest (20, 129). As discussed below, K^+ flowing through these open channels contributes a standing "silent" current that depolarizes the cells (129, 322).

The role of intracellular Ca^{2+} in adaptation has recently been questioned for mammalian hair cells (227, 228), and it has been claimed that none of the three lines of evidence already cited definitively substantiate Ca^{2+} involvement in mammalian cochlear hair cells. This conclusion is controversial (18, 48), yet there are clearly some results on adaptation in mammalian hair cells that are not explained by simple

models. Furthermore, the precise molecular mechanism of either kinetic form of adaptation remains unclear. Slow adaptation has been suggested to involve a change in the attachment point of the elastic element connected to the MET channels (118). A possible physical manifestation of this process is that during a positive bundle deflection, increased tension in the tip link causes its upper attachment point to slip down the side of the stereocilium, which reduces the tension in the elastic element and causes adaptation. At the end of the stimulus, tension is reduced, and the attachment point of the tip link is pulled back up the stereocilium by a motor ascending along the actin backbone of the stereocilium (8,118) to retension the tip link. The motor has been variously identified with myosin IC in nonmammals (97) and myosin VIIa (154) or myosin VI (183) in mammals. However, the millisecond time constant of fast adaptation argues against mediation via an ATPase as in any myosin isoform, and the speed is more consistent with the motor occurring at a site very close (<30 nm) to the MET channel (51, 245). One specific hypothesis is that adaptation stems from a Ca^{2+}-induced change in the force sensitivity of the MET channel, which makes opening the channel more difficult (40, 51). More detailed models may emerge when the full molecular structure of the MET channel complex is elucidated.

Molecular structure of the transducer channel complex

Although the structural details are still incomplete, much has been discovered over the last 15 years about the molecular organization of the hair bundle, the tip links, and their connection to the MET channel. This research has been extensively reviewed (12,80,249,318). Owing to the small number of hair cells per cochlea and the low abundance of many of the proteins (e.g., there are probably fewer than 200 MET channels per hair bundle), characterization of the hair bundle proteome using conventional biochemical experiments has proved difficult. Most information has come from studying various mutations linked to human deafness and their equivalents in mice [(231, 249); Table 1]. Genetic hearing loss presents in two

Table 1 Some Hair Bundle Proteins Mutated in Human Deafness

Protein	Human deafness	Protein type	Location
Myosin VIIa	USH1B, DFNA11	Motor	Top of tip link
Harmonin-b	USH1C, DFNB18	Scaffold. PDZ	Top of tip link
Cadherin-23	USH1D, DFNB12	Membrane protein	Tip-link component
Protocadherin-15	USH1F, DFNB23	Membrane protein	Tip-link component
Sans	USH1G	Scaffold. PDZ	Top of tip link
cib2	USH1J, DFNB48	Ca-binding protein	Top of stereocilium
Usherin	USH2A	Membrane protein	Inter-ciliary ankle links
VLGR1	USH2C	Membrane protein	Inter-ciliary ankle links
PTPRQ	DFNB84	Membrane protein	Inter-ciliary links
Whirlin	USH2D, DFNB31	Scaffold protein	Top of stereocilium
Clarin-1	USH3A	Membrane protein	Stereocilium
Myosin-IIIa	DFNB30	Motor	Top of stereocilium
Myosin VI	DFNA22, B37	Motor	Base of stereocilium
Myosin XVa	DFNB3	Motor	Top of stereocilium
Stereocilin	DFNB16	Extracellular	Top of stereocilium
Espin	DFNB36	Actin-binding	Along stereocilium
eps8	DFNB102	Actin-binding	Top of stereocilium
TRIOBP	DFNB28	Actin-binding	Base of stereocilium
Radixin	DFNB24	Actin-binding	Base of stereocilium
Taperin	DFNB79	Actin-binding	Base of stereocilium
TMC1	DFNA36, B7/11	Membrane protein	MET channel
LHFPL5	DFNB67	Membrane protein	MET channel
TMIE	DFNB6	Membrane protein	MET channel

DFNA, autosomal-dominant; DFNB, autosomal-recessive; USH, Usher syndrome; for sources see text and also http://hereditaryhearingloss.org/.

forms: syndromic and nonsyndromic. In syndromic hearing loss, deafness is associated with other phenotypes, such as blindness in Usher syndrome, while in nonsyndromic hearing loss, inner ear defects are the sole disorder. Thirty autosomal dominant genes (DFNA) and 62 autosomal recessive genes (DFNB) are currently associated with nonsyndromic hearing loss, and many of them are connected with hair bundle structure. Table 1 lists the most common ones, and the Hereditary Hearing Loss Homepage (http://hereditaryhearingloss.org/) offers a more complete set. Most of the genes in Table 1 fall into four categories: actin-binding proteins, interciliary links, MET channel components, and lower tip link density.

Figure 4D depicts current knowledge of the components of the transduction apparatus. The tip link is composed of homodimers of protocadherin-15 at its lower end and cadherin-23 at its upper end (136). Both proteins have long extracellular domains formed from multiple extracellular cadherin (EC) repeats, which interact at their N-termini in a Ca^{2+}-dependent way to generate a strand 150 nm in length (91,136). The upper end of the tip link is anchored to the stereociliary backbone by a tertiary complex of the Usher proteins myosin VIIa, sans, and harmonin-b (105). The equivalent mooring at the lower end is not fully established, but it may include whirlin (194), myosin XVa (14, 62), eps8 (182), and myosin IIIa (272). These proteins are all likely to be involved in regulating actin polymerization at the top of the stereocilium and therefore dictating stereociliary height (12, 71, 182). The lower end of the tip link, formed by protocadherin-15, is also connected to the putative MET channel components TMC1 [transmembrane channel-like protein; (78, 135, 157, 158)], LHFPL5 [previously named TMHS for tetraspan membrane protein of hair cell stereocilia; (23, 173, 312)], and TMIE [transmembrane inner ear; (98, 319)]. Protocadherin-15 falls into three isoform classes, CD1, CD2, and CD3, which have distinct carboxy termini (2,302); the CD2 isoform is the native isoform in mammalian auditory hair cells (230), and it is the only isoform thought to interact with TMIE (319).

The MET channel pore has been particularly difficult to identify, with several false leads and no obvious relationship to mechanosensitive channels in other systems or taxa (80). Currently, the best candidate is TMC1, which has six to eight transmembrane domains, similar to K^+ channel subunits (78,159), and fulfills most of the necessary criteria. First, TMC1 is localized to the stereociliary tips where the MET channels are located (23, 157), and it interacts with PCDH15 (23, 175). Second, *Tmc1* knockout eliminates MET currents later than P8, resulting in deafness and hair cell degeneration in the adult (135). A lack of TMC1 prior to P7 is compensated for by TMC2, but the latter isoform is downregulated after P7. Third, *Tmc1* mutations alter MET channel unitary conductance (23, 145, 223) and the Ca^{2+} permeability of the channel (18, 49, 146, 223). Finally, during the first neonatal week, when TMC2 is also present in mouse cochlear hair cells, *Tmc1* knockout virtually abolishes the tonotopic gradient in single MET-channel conductance (19, 23). These lines of evidence suggest that TMC1 is an essential component of the MET channel complex. However, evidence for expression of vertebrate TMC1 in a heterologous cell system, in which the protein is transported to the plasma membrane, is still lacking (78,109). Therefore, the mechanosensitivity of this membrane protein cannot be directly demonstrated, as has been done for other mechanically gated channels such as NOMPC (314) and PIEZO2 (50). TMC proteins also exist in nonvertebrates, and mutants have been studied in *Caenorhabditis elegans* (36, 317) and in *Drosophila melanogaster* (109). *Drosophila* larvae with loss-of-function mutation of tmc exhibited defective locomotion, a phenotype that could be rescued by expressing *Drosophila* TMC or mouse TMC1 and/or TMC2 in tmc-positive proprioceptive neurons. Unequivocally establishing a direct mechanosensitive role for TMC1 must await successful expression and testing of the protein in a heterologous system.

Receptor potentials in inner and outer hair cells

The MET current, principally carried by K^+ ions with a minor contribution from Ca^{2+}, enters the hair cell across the hair bundle membrane and leaves via the basolateral membrane. There are no action potentials in mature cochlear hair cells (152), but several types of voltage-dependent K^+ channel in the basolateral membrane contribute to the resting potential and shape the receptor potential. The types of K^+ channel that are present differ between OHCs and IHCs and also change with neonatal development. After P8, the dominant K^+ conductance in OHCs is G_{Kn}, which is composed of KCNQ4 subunits that are upregulated in parallel with the appearance of the motor protein prestin and acquisition of electromotility (187). Mature IHCs after P12 possess two main voltage-dependent K^+ conductances, one with slow activation kinetics G_{Ks} and the other with fast kinetics G_{Kf}, in addition to a small amount of KCNQ4 (152, 153, 184). In OHCs, G_{Kn} is activated at unusually negative membrane potentials, with half-activation near −65 mV, so it may be fully turned on at the resting potential (129).

Owing to the low Ca^{2+} concentration in endolymph bathing the hair bundles coupled with the millimolar intracellular calcium buffer concentration in OHCs (110), the MET channels in those hair cells are half open at rest (p_{OR}, probability of MET channel opening at rest ~0.5). Consequently, there is a large resting inward current flowing into the hair cell, which is known as the "silent" current (129, 322). The OHC resting potential is determined by the balance between the depolarizing transducer current and the hyperpolarizing KCNQ4-based I_{Kn} (Fig. 8). It has been estimated that they together generate a resting potential of −45 to −50 mV *in vivo* (129), which mid-way between the K^+ equilibrium potential and the MET channel reversal potential. Because the MET channels are half-open at rest, a sinusoidal displacement of the hair bundle will evoke a corresponding sinusoidal voltage excursion around the resting potential, with the MET channels closing on one half cycle of the stimulus and opening on the other half cycle. This form of receptor potential will extend to high frequencies, and it will be limited only by the fact that the

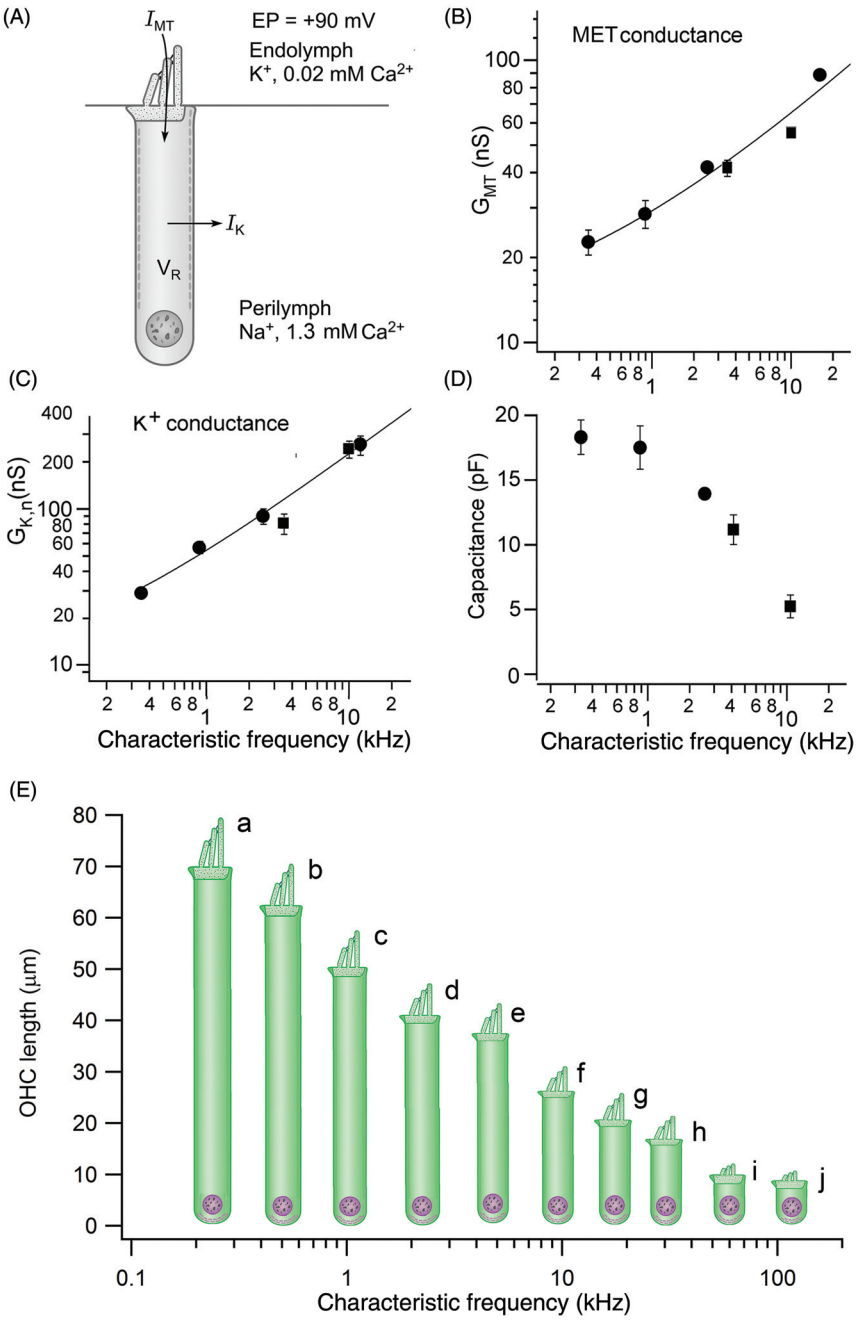

Figure 8 Tonotopic variations in membrane properties of rodent outer hair cells. (A) Principal membrane currents determining potential of outer hair cell. MET current, I_{MT}, carried mainly by K^+ ions, flows in through MET channels down a potential gradient determined by the positive endolymphatic potential (EP, 90 mV) and the resting potential (V_R, ~ −50 mV); the K^+ current exits mainly via GK,n channels in lateral wall, down a K^+ concentration gradient into the perilymph. (B) MET conductance, G_{MT}, increases with the characteristic frequency at the location of the hair cell. (C) Voltage-dependent K+ conductance, GK,n, increases with hair-cell characteristic frequency. (D) Membrane capacitance decreases with hair-cell characteristic frequency, signifying a progressive decrease in the size, mainly the length, of the outer hair cell. Combining results in B, C, and D, implies a significant reduction in the membrane time constant determined by $C/(G_{MET} + G_{Kn})$. Results are combined measurements from gerbils (filled circles) and rats (filled squares) and were taken, with permission, from (129). (E) OHC length (and hence membrane area and electrical capacitance) decreases with increase in characteristic frequency in different mammals: (a) chinchilla, human; (b) guinea pig; (c) chinchilla, gerbil; (d) guinea pig, chinchilla; (e) gerbil, rat; (f) chinchilla, mouse, rat; (g) guinea pig, rat, human; (h) rat, bat; (i) mouse; (j) bat. Data, with permission, from [(60); rat, bat, guinea pig, and gerbil], [(25); chinchilla], [(235, 239); human], and from author's laboratory (rat, mouse, and gerbil).

membrane behaves as a low-pass filter with corner frequency, $F_{0.5}$, set by the membrane time constant, τ, where $F_{0.5} = 1/2\pi\tau$. The time constant can be calculated from the resting conductance, G [$G = (G_{MET} + G_{Kn})_{REST}$, where G_{MET} and G_{Kn} are the conductances of the MET channel and the KCNQ4 K^+ channel (both specified in the resting state)], and the membrane capacitance, C ($\tau = C/G$). The smaller the membrane time constant, the higher the corner frequency, $F_{0.5}$, before the sinusoidal receptor potential is attenuated. Since MET and KCNQ4 conductances increase along the cochlea's tonotopic axis and cell capacitance decreases (129, 180), the membrane time constant decreases from the low-frequency to the high-frequency end of the cochlea (Fig. 8). The cochleotopic gradient in OHC plasma membrane properties allows sinusoidal modulation in membrane potential up to high frequencies (>10 kHz), and as discussed later, the gradient will facilitate activation of the motor protein prestin on a cycle-by-cycle basis at these frequencies.

IHCs have a much lower concentration of cytoplasmic calcium buffer compared with OHCs, and consequently their MET channels are only marginally open at rest (p_{OR} ~0.05) and the standing MET current is small. Therefore, the resting potential of IHCs is −60 mV (130), which is nearer to the K^+ equilibrium potential. Thus the MET current and the receptor potential in IHCs are both asymmetric, with a larger depolarizing component on one-half cycle than the hyperpolarizing component on the other half cycle. This situation is referred to as rectification by analogy with an electrical circuit element that permits current flow in one direction but not the reverse. When the stimulation frequency exceeds $F_{0.5}$, the periodic component will be attenuated or filtered out, leaving a sustained depolarization often referred to as the summating potential. The transition from periodic receptor potential to sustained depolarization in IHCs occurs at a corner frequency, $F_{0.5}$, of approximately 2 kHz (Fig. 9C). Provided a rate-limiting step is not imposed by the time course of synaptic exocytosis, a corner frequency of 2 kHz will allow phase-locking in the auditory nerve discharge up to this frequency (Fig. 9D). The two types of K^+ channel in IHCs will also shape the receptor potential, especially the summating potential seen at higher frequencies. The onset of the summating potential will be limited by the membrane time constant. With louder sounds evoking larger receptor potentials, the membrane time constant will be reduced due to voltage-dependent activation of G_{Kf}, which will thus accelerate the voltage onset [Fig. 9A; (153)]. G_{Ks} by comparison will contribute a slow adaptation to the summating potential that will more pronounced with larger responses.

As with assigning roles to the constituents of the mechano-electrical transduction apparatus, genetic manipulations have been used to assess the physiological contributions of the hair cell K^+ channels. I_{Kf}, the fast K^+ current in IHCs, is thought to flow through ion channels equivalent to large-conductance (BK) Ca^{2+}-activated K^+ channels (185) that are clustered around the neck of the IHC (236). G_{Kf} channels are primarily voltage gated and minimally modulated by Ca^{2+} influx (probably because the Ca^{2+} channels lie at some distance from the neck of the IHC). G_{Kf} channels, unlike the BK channels in non-mammalian hair cells, do not underlie an electrical resonance of the type seen in non-mammals (79). Knocking out the BK alpha subunit (*Kcnma1*$^{-/-}$) in mice had a minimal effect on hearing (237). The main consequence was a reduced precision in the timing of action potentials in auditory nerve firing, which was reflected by an increased variance of first spike latency in response to tone bursts (219). This impairment could be explained by a slower onset to the IHC receptor potential resulting from a smaller fast-activating K^+ conductance (G_{Kf}). In contrast with the minor effect of mutating BK channels in IHCs, the outcome of mutating the KCNQ4 channel in OHCs is more profound and is linked to the non-syndromic deafness DFNA2. A number of missense or deletion mutations have been described. These mutations produce human hearing loss that can affect all frequencies or can be confined to high frequencies (211). In *Kcnq4*$^{-/-}$ mice, a progressive hearing loss developed in conjunction with absence of the G_{Kn} and degeneration of OHCs (142); little effect was seen on IHCs. Lack of G_{Kn} caused chronic depolarization of the OHCs because it removed the hyperpolarizing driving force opposing the resting inward current through the MET channels. Chronic depolarization has been suggested to lead to impaired cochlear amplification and slow degeneration of the hair cells (142), conceivably by Ca^{2+} overload.

Frequency Tuning

Cochlear frequency selectivity

Aside from converting acoustic stimuli into electrical signals, the auditory organ or cochlea has a second role in separating the frequency constituents in the incoming sound stimulus. It essentially performs a Fourier analysis on the waveform, so the relative amplitudes of the different frequencies can be signaled to the brain. Two distinct tuning mechanisms are employed in nonmammals and mammals. In nonmammalian vertebrates, such as the turtle, frog, and chicken, activation of BK (large-conductance) Ca^{2+}-activated K^+ channels by depolarization and an increase in Ca^{2+} following its influx through adjacent voltage-sensitive Ca^{2+} channels generates a sharply tuned resonance that filters the receptor potential (54, 79, 121). Because the resting potential is positive to the K^+ equilibrium potential (E_K), a negative feedback process exists: depolarization opens K^+ channels, which draws the membrane potential negative toward E_K. In response to an extrinsic current step, the hair cell membrane potential in lower vertebrates does not display exponential growth and decline dictated by the membrane time constant (which is determined by the product of membrane resistance and capacitance), but it instead creates damped voltage oscillations indicative of a resonator. If the resonance is regarded as the consequence of a negative feedback process, increasing the size and the speed of the feedback should theoretically increase the resonant frequency. Patch-clamp recordings from single hair cells have

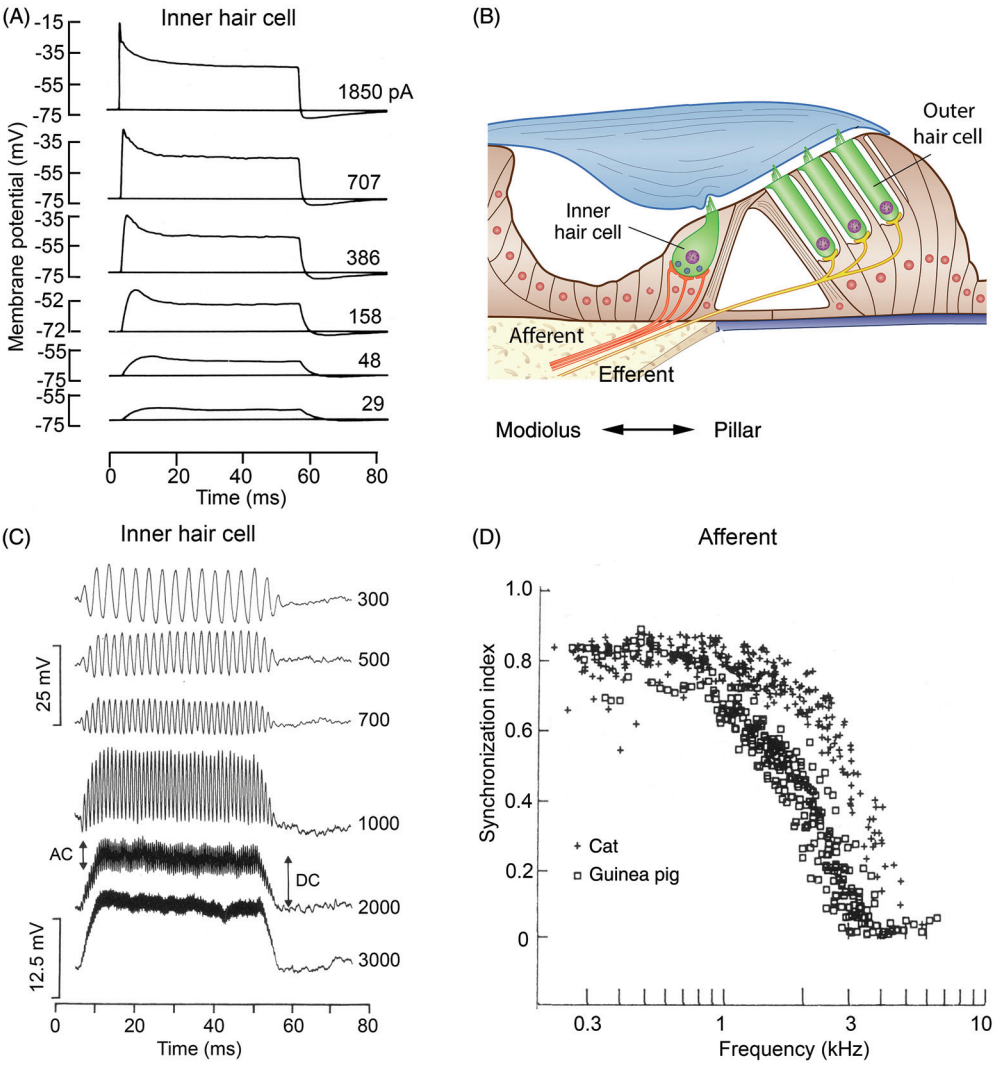

Figure 9 Filtering of receptor potentials by inner hair cell. (A) Changes in IHC membrane potential elicited by current pulses of magnitudes given next to each trace in isolated guinea pig inner hair cell. Note the voltage inactivation for larger responses. (B) Schematic of organ of Corti showing the IHC and innervation by multiple afferents. The medial and lateral sides of the IHC are often referred to as "modiolar" and "pillar," the orientation of which is shown beneath the schematic. (C) Receptor potentials in an inner hair cell of an anesthetized guinea pig for tones of different frequencies, given in Hz alongside the traces. At low frequencies, the response is purely sinusoidal, reflecting the sound stimulus. At frequencies above 1000 Hz, the periodic (AC) component is filtered by the membrane time constant leaving a sustained depolarizing (DC) component. (D) Synchronization index, indicating phase-locking in auditory nerve discharge, as a function of the frequency of the sound stimulus in auditory nerve fibers of cats (crosses) and guinea pigs (filled and open squares). An index of 1.0 denotes perfect synchronization of the spikes to a specific phase on every cycle of the tone, whereas an index of 0 denotes no relationship between the spike firing and the sound cycle. Records in (A) modified, with permission, from (153) and (C) and (D), with permission, from (222). See also Figure 14 for examples of phase locking.

demonstrated that varying the number of Ca^{2+} channels and the density and kinetics of the BK channels produces different resonant frequencies; these properties vary systematically along the auditory papilla to generate a tonotopic map [Fig. 10; (5,246)]. The applicability of the electrical resonance is limited by the fastest kinetics and densities achievable for the Ca^{2+} and BK channels, and the two channel parameters set the upper frequency range of the resonance to be at most 5 kHz in birds (284, 310). However, in mammalian evolution, selective pressure has pushed the upper frequency limit well beyond 5 kHz, which has necessitated the acquisition of a new frequency-selective mechanism. The new mechanism can handle frequency limits up to ~70 kHz in mice (283) and even higher in some bats and marine cetaceans (77).

In mammals, each sound frequency generates a traveling wave on the basilar membrane, propagating from base to apex and growing in magnitude until it peaks at the place specific

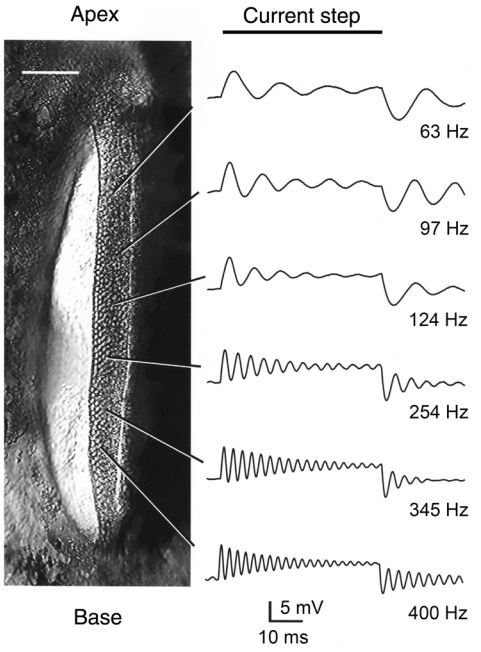

Figure 10 Tonotopic organization of the turtle auditory papilla. *Left*, medial view with the hair-cell papilla on the right-hand side of the basilar membrane; scale bar = 100 µm. *Right*, examples of electrical resonance in hair cells at different positions along the epithelium. Resonant frequency, given beside traces, increases from apex to base. Each record is the voltage response to a small depolarizing current step, the timing of which is shown at top; cells had resting potentials in the range −44 to −51 mV. Figure taken, with permission, from (246).

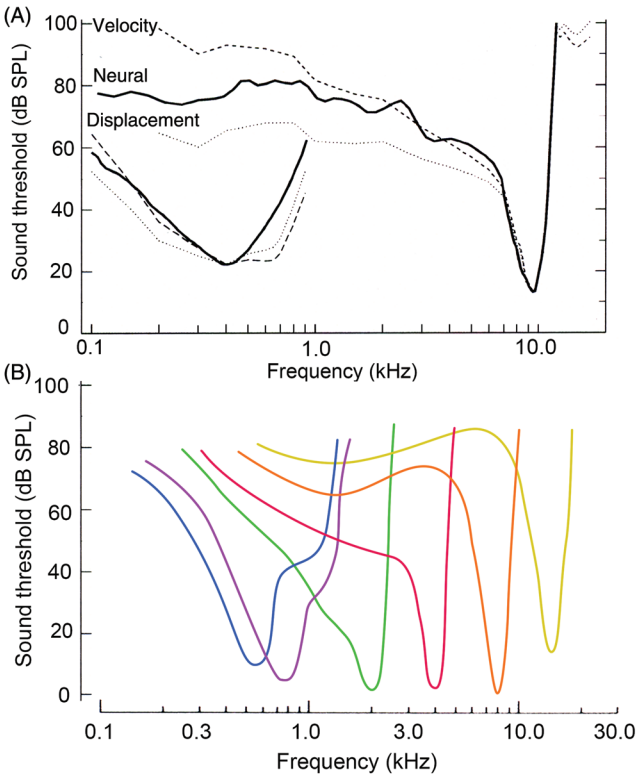

Figure 11 Mechanical and electrical tuning curves in the mammalian cochlea. (A) Solid curves are frequency-threshold tuning curves for two auditory nerve fibers in the chinchilla cochlea, with characteristic frequencies of 0.4 and 9.5 kHz. Superimposed on each nerve-fiber tuning curve at similar locations are the basilar membrane vibrations: iso-displacement response (dotted curves, 1-nm left and 2.7 nm right) and isovelocity response (dashed curves, 2.5 µm/s left, and 164 µm/s right). The results indicate almost all of the frequency tuning is present in the basilar membrane vibrations, with isovelocity responses giving better fits to the nerve fiber frequency-threshold curve; from (254). (B) Schematic of auditory nerve fiber tuning curves for the cat cochlea based on results in references (125, 165). Similar sets of tuning curves are also available for other mammals including the Mongolian gerbil (215) and the mouse (283).

for that frequency (13). Gradations of stiffness and mass of the cochlear partition along its length [(73, 134, 203, 287); reviewed in (204)] produce an exponential frequency map, with high frequencies generating the largest vibrations at the base of the cochlea and low frequencies propagating to the apex. The original measurements experimentally establishing this tonotopic organization were performed on human cadavers (13). However, the experiments were subsequently refined by applying more sensitive methods, such as Mössbauer spectroscopy (242, 274), laser interferometry [(44-46, 305); reviewed in (254)], and more recently optical coherence tomography (38, 160), to accurately determine mechanical tuning curves in living animals. The difficulties of measuring nanometer displacements of the basilar membrane in live preparations were overcome, and experiments ultimately revealed sharp mechanical frequency selectivity comparable to the frequency-tuning curves of single auditory nerve fibers (Fig. 11). The frequency-tuning curves are V-shaped functions of sound frequency. At their tip, they have a minimum response threshold at the characteristic frequency (CF) of that cochlear location or nerve fiber. At a given position, the frequency tuning in the basilar membrane vibration, at the input to the hair cells, has the same shape as that in the auditory nerve fiber discharge at the output of the IHCs (208, 275). Basilar membrane displacement provides a reasonable agreement with the nerve fiber tuning curve, but membrane velocity gives a slightly better fit, suggesting there is a high-pass filter prior to excitation of the IHCs. Such high-pass filtering might arise because the IHC hair bundles are deflected by fluid flow in the sub tectorial space rather than by deformation of the organ of Corti (57, 86, 214). The contribution of a high pass filter might be especially relevant at the cochlear apex, where the mechanical tuning curves can agree less well with the nerve fiber tuning curves. It has been claimed that at the apical location, the band pass shape inferred for mechanical tuning may be an artifact of opening the cochlea, and if the compartment is kept closed, a purely low pass mechanical tuning curve is measured (66). There may be differences in the strategies used to process low-frequency sounds at the apex compared with high frequency sound at the base. However, motion of the basilar membrane at both positions has demonstrated nonlinearity and an enhanced sensitivity for sound stimuli near the behavioral threshold. (46, 254). At the base, the enhanced sensitivity required the presence of intact OHCs. Consistent with this idea, abolition of the EP by the

diuretic furosemide, which reduces OHC receptor potentials, reversibly altered sound-evoked responses of the basilar membrane, with the greatest reduction occurring at low levels around the CF (259).

These observations can be incorporated into a scheme in which there is an initial broad passive mechanical resonance attributable to the stiffness and mass of the cochlear partition. This resonance is followed by OHCs pumping energy with each cycle into the cochlear partition, thus boosting its motion near the threshold. The active second process, often referred to as the cochlear amplifier (61), is metabolically sensitive and nonlinear. Whether power amplification exists has been contested (290), but at low sound levels, the process confers a 40 to 60 dB (100- to 1000-fold) increase in sensitivity at frequencies around the CF; at higher sound levels, the process saturates, sensitivity diminishes, and tuning broadens. Both modeling and mechanical measurements indicate that, to be most effective, the energy for amplification is injected over a short section of the cochlea basal to the peak of the traveling wave (67, 82, 277). Recordings of threshold tuning curves of auditory nerve fibers, coupled with injection of horseradish peroxidase at given locations, has demonstrated systematic variation of CF with position, often referred to as the place-frequency map, in a variety of animals including cat (167), rat (200), Mongolian gerbil (201) and mouse (202).

Mechanisms of amplification

Two OHC mechanisms have been proposed to underlie cochlear amplification and its adjuncts, sharp frequency tuning and nonlinearity near threshold. These mechanisms are hair bundle motility, which is mediated by gating of the MET channels, and somatic motility (contractions and elongations of the cell body), which is driven by voltage-dependent conformational changes in the piezoelectric membrane protein prestin. Extensive evidence exists for active hair bundle motility as a force generator in hair cells of nonmammals, including turtle (55, 243), frog (119, 191, 192), and chicken (22). Active hair bundle motility is proposed to reflect a bidirectional coupling between tip-link tension and MET channel gating. Thus, increased tension opens the channels, but conversely, channel closure, as occurs in adaptation, exerts a force on the tip link that may move the bundle. However, experimental evidence for this mechanism in mammalian cochlear hair cells is much weaker (33, 139) compared with that for somatic motility. It was known for some time (7, 32) that solitary OHCs contracted rapidly by as much as 4 percent of their length (e.g., 1 μm for a 25-μm-long cell) when depolarized by a patch electrode (Fig. 12). Electromotility of the OHC soma behaves in a similar manner to a voltage-dependent conductance, and it can be described by a single Boltzmann relation with a half-activation voltage and slope factor of approximately −50 and 30 mV, respectively (6). When length changes are minimized, each cell is able to generate an isometric force of 0.1 nN/mV (124). The membrane potential at which electromotility is half-activated is comparable to the OHC resting potential [−45 to −55 mV; (129)] so that, for small stimuli, the motor operates at a membrane potential of maximum sensitivity. The cylindrical OHC resembles a miniature muscle fiber, but its contractions are much faster than those of muscle, and the cells can undergo cyclical length changes at frequencies up to 80 kHz (84). This speed is essential if the process is to generate force on each cycle of a sound stimulus that in some mammals extends up to 100 kHz, which is near the upper frequency limit of hearing in several mammalian genera such as mice and bats. This impressive speed highlights that the underlying mechanism cannot involve an actomyosin mechanism controlled by ATP like that found in muscle fibers (115).

The membrane protein underpinning electromotility was cloned by subtractive hybridization based on its expression in OHCs but not in IHCs. The protein was named prestin after the musical term *presto* (i.e., quick tempo), and it was shown to be a member of the solute transporter family SLC26A5 (320). Indeed, prestin orthologs in nonmammals such as zebrafish and chicken can function as electrogenic anion exchangers, but this transport mechanism is largely lost in mammalian prestin (268). However, the anion binding retains significance as demonstrated by the observation that electromotility attributable to prestin required intracellular Cl^- (or HCO_3^-) ions, and removal of these ions abolished motility [Fig. 12; (218)]. The hypothesis that Cl^- binding might account for the voltage dependence has not been unequivocally verified so far, although recent structural observations have hinted at the binding site (101). Conclusive evidence on the importance of prestin for cochlear amplification was obtained from its genetic deletion in mice, which caused loss of electromotility in isolated OHCs and 50 dB reduction in cochlear sensitivity *in vivo* (169). This finding was criticized, however, because the absence of prestin substantially reduced the stiffness of the hair cells and of the organ of Corti. Prestin is normally packed in the OHC lateral membrane at an enormously high density of over 10,000/μm^2 (113, 176), and the sensitivity might therefore have been diminished as a result of the reduction in stiffness. To address this criticism, another approach was devised. A mutant mouse with a nonfunctional prestin (V499G/Y501H) was created, but the mutated protein was nevertheless still targeted to the OHC lateral membrane so cellular stiffness was unaltered. Isolated OHCs from this mutant had much reduced electromotility and 60 dB loss of acoustic sensitivity *in vivo* (59). Taken together, the genetic manipulations argue that OHC electromotility based on prestin underlies the majority of cochlear amplification. Further support for this conclusion came from the observation that changes in chloride concentration that would block OHC contractions when applied to the perilymph *in vivo* produced substantial reduction in cochlear amplification without affecting forward mechanotransduction (267).

A problem with somatic motility is that it is not immediately clear how prestin can be activated on a cycle-by-cycle basis at the frequencies of tens of kilohertz used by many mammals; in theory, the receptor potential driving the prestin

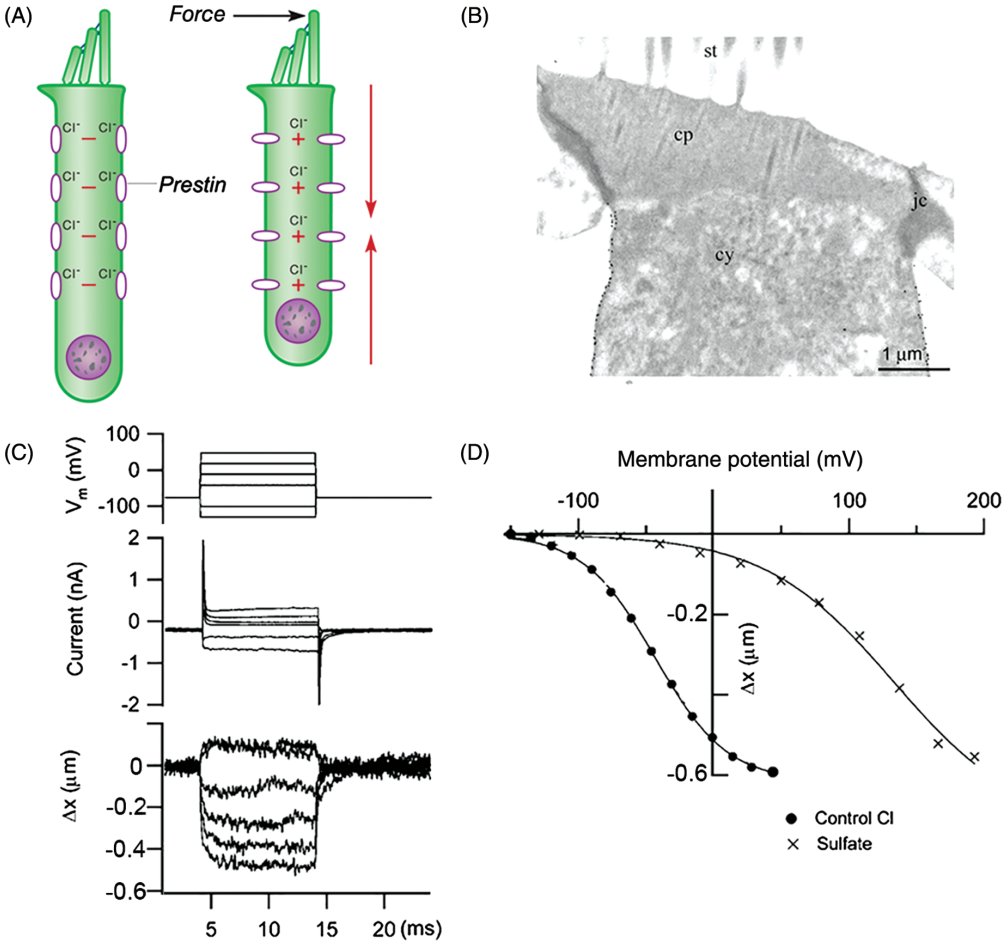

Figure 12 Outer hair cell contractility mediated by prestin. (A) Schematic of outer hair cell with prestin molecules in lateral wall. Force applied to hair bundle open MET channels, causing depolarization and cell contraction due to change in conformation of prestin. (B) Transmission electron micrograph of rat outer hair cell immunolabeled for prestin shows gold particles in the lateral wall; abbreviations: st, stereociliary bundle; cp cuticular plate; cy, cytoplasm; jc junctional complex. (C) Contractions of outer hair cell evoked by voltage steps from −120 mV to +50 mV; length change measured with dual photodiode; (D) plots of length change in outer hair cell recorded with chloride-based and sulfate-based intracellular solutions. With chloride, the prestin was half-activated at −50 mV, but sulfate shifted the activation relationship ~150 mV positive. B taken, with permission, from (176); C and D taken, with permission, from (141).

switch should be filtered by the millisecond time constant of the OHC membrane (117). This discrepancy fueled the notion that hair bundle motility, as an alternate mechanism, could generate the necessary force at high frequencies, mainly because force production with hair bundle motility was potentially very fast and limited only by the kinetics of MET channel gating. Although some experiments have shown that active hair bundle movements synchronized to channel gating can be evoked in mammals as in nonmammals (33, 139), it seems unlikely that these movements make a major physiological contribution. The maximum bundle force that can be produced by hair bundle motility (~50 pN) is 100-fold less than that generated by prestin (5 nN) (204). Furthermore, cochlear modeling has indicated that active hair bundle forces alone are insufficient to power high-frequency cochlear amplification (196). Nonetheless, it is conceivable that the alternate hair bundle motility mechanism may operate at low frequencies.

The limit on somatic motility imposed by the membrane time constant, τ_m, has been reassessed, and extrapolations to more physiological conditions have suggested that the OHC cutoff frequency ($F_{0.5} = 1/2\pi\tau_m$) may be substantially higher than originally proposed (129, 205). Both membrane conductances, G_{MET} and G_{Kn}, were found to increase, and cell capacitance, C_m, decreased with CF in OHCs (Fig. 8); at body temperature, membrane time constants as short as 25 µs were predicted (129). The experiments to determine OHC time constants were performed on rats and gerbils, with results being collected on cells with CFs below 15 kHz and extrapolated to higher frequencies. However, it is not known whether the reduction in membrane time constant extends to the very high frequencies of 100 kHz used in ultrasonic hearing in some species of bats and in cetaceans such as dolphins and whales. It has also been argued that OHC membrane cutoff frequencies may be considerably higher when

these cells are embedded in the organ of Corti than in isolated hair cells (198, 238). Both experimental measurements and modeling indicate that somatic motility alone may therefore be adequate to produce cochlear amplification and sharp frequency selectivity throughout the mammalian frequency range.

Displacement and deformation of the organ of Corti

The steps involved in hair cell excitation can be summarized as follows. On the negative (rarefaction) phase of a pure tone stimulus, the basilar membrane and organ of Corti are drawn upward toward the scala vestibuli (Fig. 13), which causes a shearing motion between the reticular lamina and the tectorial membrane. The tectorial membrane is tightly attached to the OHC hair bundles, and its radial motion deflects the bundles abneurally in the excitatory direction, thereby opening MET channels (Fig. 13A). The resultant depolarizing receptor potential activates prestin, causing OHC contraction, which in turn compresses the organ of Corti, pulling the basilar membrane and reticular lamina together (Fig. 13B). Opposing movements of the basilar membrane and reticular lamina have been observed experimentally when electrical stimuli were applied to the organ of Corti in a temporal bone preparation (181); these movements imply a complex deformation of the organ of Corti resulting from OHC contraction. At the high-frequency base, the reticular lamina is less stiff than the basilar membrane (171) and so undergoes a larger displacement, as has been demonstrated with *in vivo* optical coherence tomography (38). This mechanical feedback may produce amplification if it is applied with appropriate timing relative to the acoustic stimulus, but the timing of the mechanical steps is controversial. An additional factor that in theory might influence the deformation of the organ of Corti (and amplification) is the unusual Y-shaped structure formed by the OHCs and the phalangeal processes of the Deiters' cells, the heads of which intercalate with the tops of the OHCs in forming the continuous sheet known as the reticular lamina. The OHCs are tilted longitudinally toward the base of the cochlea, whereas the phalangeal processes of the Deiters' cells are tilted in the opposite direction, toward the apex. These two structures have been proposed to generate a push-pull action: the OHCs, when contracting, produce a feed-forward action, and the Deiters' cell phalangeal processes tilt to a feedback action. These movements cooperate for short wavelengths, boosting traveling waves propagating toward the apex, but they cancel out for long wavelengths (93, 316). Therefore, the notion that when the basilar membrane is deflected, the organ of Corti moves like a "rigid body" is incompatible with OHC somatic motility. Recent experimental and theoretical attempts to understand the relative electromechanical interactions within the organ of Corti [references (67, 134, 160, 205, 241, 316)] are a collective effort to establish a new theory to accommodate the OHC motility. Nevertheless, although it is generally agreed that the organ of Corti cannot be considered a rigid body, little consensus exists on the magnitude and phase relations of the interactions as it deforms.

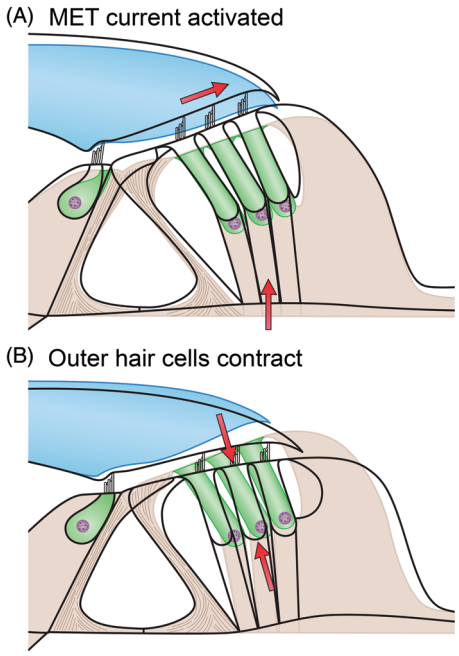

Figure 13 Deformation of organ of Corti during stimulation. (A) Excitatory (rarefaction) sound stimulus causes upward deflection of basilar membrane and organ of Corti. On conventional view, the entire organ moves upward without changing shape and causes abneural displacement of hair bundles; brown background denotes resting position and black outline new stimulated position. (B) Electrical stimulation elicits contraction of outer hair cells and compression of the organ of Corti, with the reticular lamina being pulled down and basilar membrane pulled up. During normal stimulation it is envisage that both processes in A and B will occur sequentially but the exact timing is still uncertain.

Another knowledge gap exists for the mechanisms of amplification and tuning at the low-frequency apex. Most of the available results were garnered by imaging, using an approach through the round window at the base of the cochlea. It has been difficult to measure basilar membrane motion *in vivo* at the apex, especially in animals such as the guinea pig and chinchilla that have a hearing range that extends below 1 kHz (66). The frequency range less than a few kilohertz is of interest because it is correlated with a change in the shape and symmetry of the auditory nerve fiber tuning curves, with secondary peaks, in both cat and chinchilla [Fig. 11B; (125, 165, 285)]. These and other observations have led to the suggestion that a different tuning mechanism may operate at the cochlear apex (286, 292); indeed, the apex might be the one cochlear region where active hair bundle motility makes a significant contribution (240). At the very least, deformation of the organ of Corti by OHC contractions is likely to differ at the apex. The basilar membrane there, unlike that at the base, is thought to have a stiffness comparable to that of the reticular lamina; therefore, during OHC contraction the two structures undergo displacements of similar magnitude but opposite polarity (171, 204).

Tectorial membrane

The relative shearing motion of the tectorial membrane is believed to produce fluid flow in the subtectorial space (between the underside of the tectorial membrane and the reticular lamina), which can drive the IHC hair bundles. However, the exact contribution of the tectorial membrane is not fully understood mainly because, unlike the basilar membrane and reticular lamina, it is difficult to image *in vivo*. Recent optical coherence tomography measurements have suggested the tectorial membrane carries a second layer of traveling waves distinct from that along the basilar membrane (160). It is conceivable that the mass and stiffness of the tectorial membrane, together with the OHC hair bundle stiffness, generate an auxiliary resonance that can modify the tuning of mechanical stimuli into the IHC (108, 323). The stiffness of both the tectorial membrane (251) and the OHC hair bundles (21) increase in progressing toward the base of the cochlea. Taken together, these changes could in theory raise the resonant frequency.

Further evidence about the role of the tectorial membrane has been derived from mutations in its structural elements. The membrane is an acellular gel composed of a glycoprotein matrix of α-tectorin and β-tectorin in which collagen fibrils that course radially are embedded (250). The orientation of the collagen fibers makes the membrane anisotropic, with strong radial coupling across the three OHC bundles and weaker longitudinal coupling along the cochlea. Targeted deletion of α-tectorin caused loss of the collagen matrix and detachment of the tectorial membrane from the top of the organ of Corti; this resulted in a 100-fold reduction in acoustic sensitivity and complete loss of amplification (161). In a similar manner, deletion of β-tectorin also produced a reduction in acoustic sensitivity, but this reduction was accompanied by an enhanced sharpness of mechanical tuning (262). This surprising result has been ascribed to a reduced longitudinal coupling of the tectorial membrane that caused the tuned vibrations to be narrower and less distributed (95, 132, 195). CEACAM-16 is a third glycoprotein in the tectorial membrane, and it is thought to interact with both α-tectorin and β-tectorin. In the absence of CEACAM-16, there is loss of the striate-sheet matrix but an increase in activity, as indicated by spontaneous otoacoustic emissions (37). This observation supports a role for the tectorial membrane in the mechanical sensitivity and stability of the cochlea. Cochlear amplification in the mammal may therefore be regarded as an emergent property of complex mechanical interactions across the cochlear partition.

Signal Transmission

Inner hair cell afferent synapse

The IHCs are the sensory receptors through which most of the cochlear output is relayed. In mature hearing mammals, 95 percent of the auditory afferent neurons, the type I radial fibers with myelinated axons and cell bodies in the spiral ganglion, synapse on IHCs. In contrast, OHCs receive the residual 5 percent, the thin type II unmyelinated afferent fibers (89). Sound-evoked receptor potentials in IHCs are modulations in membrane potential around rest resulting from vibrations of the hair bundles. At low sound frequencies, the receptor potential waveform matches the sound stimulus, but at frequencies above a few kilohertz, it transforms into a sustained depolarization as the periodic component is attenuated by the membrane time constant (Fig. 9C). These two forms of receptor potential—one synchronized with the sound and the other summating—are manifest in the auditory nerve fiber spike discharge. This discharge is phase-locked to the cycles of the acoustic stimulus at low frequencies (Fig. 14), but it changes to a sustained increase in firing at frequencies above ~2 kHz (144, 255).

All sound-evoked spike responses are superimposed on a resting spontaneous activity (i.e., a continuous random firing of action potentials) generated by spontaneous excitatory postsynaptic potentials (EPSPs; Fig. 14). The spontaneous firing displays wide heterogeneity between fibers, with almost no discharge in some fibers and up to 100 spikes/s in others (165). Studies, first in cats and subsequently in other mammals, have revealed a correlation between the spontaneous discharge rate and the acoustic threshold or sensitivity. Fibers having low sound threshold (greatest sensitivity) are accompanied by a high spontaneous firing rate, and those with high threshold (low sensitivity) have low spontaneous rates (165). Each IHC receives 10 to 20 nerve terminals, which together encompass the entire spectrum of spontaneous activity. High sensitivity and spontaneous rates have been linked with large-diameter mitochondria-filled fibers synapsing on the lateral side of the IHC abutting the inner pillar cell. Fibers with low sensitivity and spontaneous rate correspond to thinner fibers contacting the medial side of the IHC facing the spiral ganglion which is embedded in the modiolus (166) and is often referred to as the modiolar side (Fig. 9B, Fig. 15). This pattern is an important feature of the innervation, and one of its functions may be to extend the dynamic range of the output.

The properties of synaptic transmission between hair cells and auditory nerve afferents has been analyzed in patch-clamped cells, mainly by monitoring changes in membrane capacitance as an indicator of exocytosis (24, 270). A difficult but more direct approach has been to simultaneously record from both presynaptic and postsynaptic cells (103, 137). The latter method has also been used to corroborate the capacitance technique (162). From such recordings, it has been found that the IHC releases the neurotransmitter glutamate which acts on postsynaptic AMPA (α-amino-3-hydroxy-5-methyl-4-isoxazolepropionic acid) receptors that can be blocked by CNQX (99, 137). However, the synapse possesses several functional properties that differ from most other glutamatergic synapses in the central nervous system. There are three principal differences. First, the presynaptic signal is a graded change in membrane potential rather than an action potential, and synaptic output must be graded with depolarization; in adults, there is a linear relationship between the

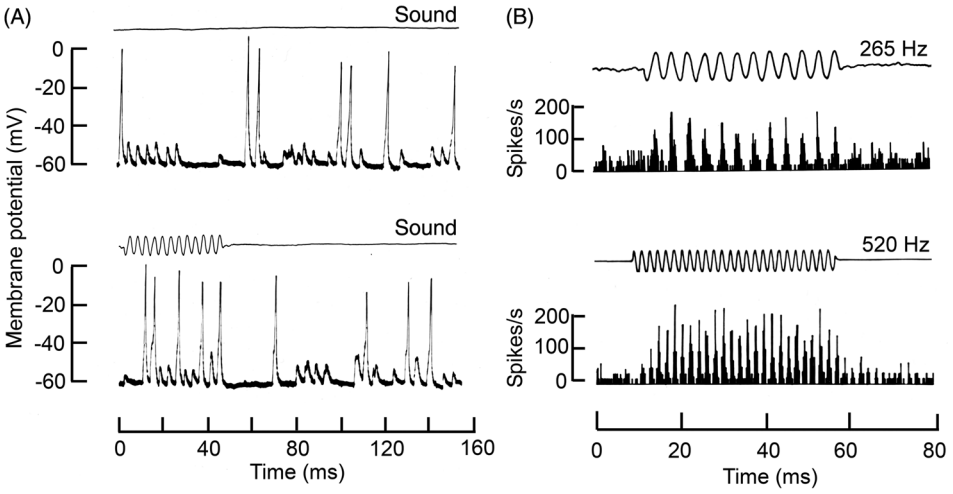

Figure 14 Synaptic potentials and action potentials in an auditory afferent. (A) Microelectrode recordings from an auditory nerve terminal in the turtle cochlea showing the spontaneous synaptic potentials and action potentials in the absence of a sound stimulus (top) and the response evoked by a tone at 265 Hz, 54 dB SPL (bottom). (B) Peristimulus histograms showing phase locking of action potentials to a 265 Hz tone (top) and a 520 Hz tone (bottom) from cell in (A); modified, with permission, from reference (53).

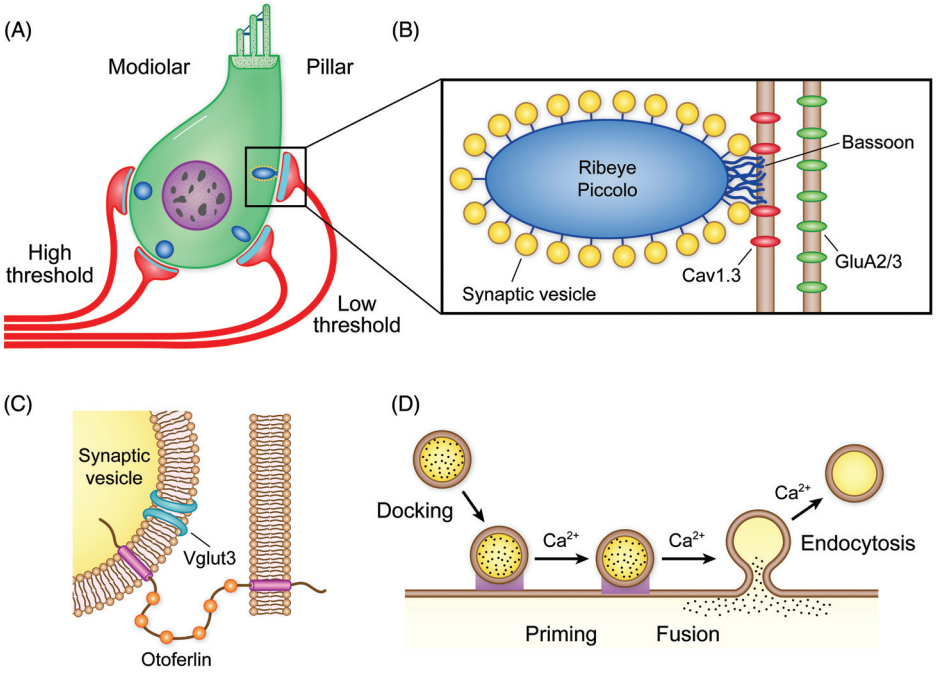

Figure 15 The synapse between the inner hair cell and cochlear afferent fiber. (A) Inner hair cell makes synaptic contacts with multiple (10-20) afferent fibers on its basolateral aspect, each synapse having one presynaptic ribbon (blue) and release site onto one afferent. Fibers synapsing on the pillar side are thought to have low thresholds and high resting spontaneous firing; fibers synapsing on the modiolar side have high threshold and low spontaneous discharge. The ribbons are smaller and the postsynaptic glutamate receptor densities (blue strip) are larger for the low threshold fibers. (B) Enlargement of the (blue) ribbon surrounded by halo of (yellow) synaptic vesicles. The ribbon is composed of ribeye and piccolo proteins and anchored to the membrane of the release site by bassoon. Vesicles are exocytosed by Ca^{2+} influx through Cav1.3 Ca^{2+} channels on presynaptic membrane and glutamate neurotransmitter binds to GluA2/3 receptors on the postsynaptic membrane. (C) High power view of synaptic vesicle, glutamate transporter Vglut3, and Ca^{2+} sensor otoferlin with six C2 domains. (D) Conventional view of the life cycle of the synaptic vesicle, from docking at the release site, interaction of vesicular and target SNARE proteins and priming for release, fusion and reuptake. Several of these processes are thought to be Ca^{2+}-sensitive and possibly mediated by otoferlin.

presynaptic Ca^{2+} influx and the postsynaptic current (137). Second, for prolonged stimuli, there is a tonic release of neurotransmitter without rundown or depression, with the synapse being referred to as indefatigable (271); at some synapses, a persistent high spontaneous release of neurotransmitter may also occur. Third, synaptic transmission must possess a submillisecond temporal precision and phase constancy to account for accurate phase locking of the nerve spike activity. Thus, for trains of sinusoidal IHC stimuli, the excitatory postsynaptic currents (EPSCs) are elicited at a constant phase of each cycle irrespective of the stimulus intensity (102). This temporal precision is also essential for achieving responses with fast onsets to produce brief but reproducible interaural time differences as needed for spatially localizing sound stimuli. The location of a sound stimulus is partly determined from the difference in the times of arrival of the sound at the two ears. For all mammals this time difference is well under a millisecond (133). Therefore, to ensure that this calculation is accurate, the delay between the onset of a sound stimulus and the start of the spike discharge must be precise and reproducible. Based on postsynaptic recordings, the prevailing hypothesis is that the IHC synapse operates by synchronized multivesicular release (99, 162), which may be important for enabling high frequency transmission. However, how synchronized multivesicular release is achieved is unclear and an alternative proposal for generating EPSCs of different amplitudes and shapes might be that a single vesicle releases variable amounts of transmitter by flickering of the fusion pore (35).

To assess the physiology, it is useful to describe the prevailing scheme for release of neurotransmitter applicable to most synaptic terminals (34). The neurotransmitter molecules, here glutamate, are packaged into ~40-nm diameter membrane-delimited vesicles that are guided to and docked against active release sites on the plasma membrane, where a molecular complex of three SNARE proteins is assembled, readying the vesicle for fusion. SNARE is an acronym for (soluble NSF Attachment Protein) receptor, and denotes a class of proteins that mediate vesicle fusion. The SNARE complex at many presynaptic terminals comprises vesicle proteins (e.g., synaptobrevin) and plasma membrane proteins (e.g., syntaxin and SNAP-25), which colocalize with a Ca^{2+} sensor such as synaptotagmin. A complex between synaptotagmin and SNAP-25 has also been implicated in vesicle docking (199). At this stage in the release cycle, the vesicle is relatively stable in a primed state until Ca^{2+} enters via nearby voltage-dependent Ca^{2+} channels. The Ca^{2+} ions then associate with the synaptotagmin sensor and trigger fusion of the vesicle with the plasma membrane causing release of its neurotransmitter. The synaptic vesicle membrane is subsequently retrieved or endocytosed to be recycled to form a new vesicle, and restocked with neurotransmitter. The details of this scheme have been derived from observations at a number of synapses, including the calyx of Held, a large synapse in the medial nucleus of the trapezoid body that mediates fast transmission in the brainstem auditory pathway (26).

The ribbon synapse

The IHC synapse deviates in several important respects from this general model (Fig. 15). The most marked deviation is the presence of an electron-dense ovoid synaptic ribbon at the release site (often referred to as the active zone) around which the synaptic vesicles are assembled like a halo (99, 193, 263). Each ribbon in IHCs is associated with one nerve terminal, and thus each active zone marking an IHC synapse is the sole input to one spiral ganglion neuron. [This anatomical arrangement differs from that in nonmammalian turtle and frog hair cell synapses that have been studied, where many ribbon synapses converge on a single afferent (137, 270)]. Such presynaptic ribbons are present in some other sensory neurons, including retinal photoreceptors and bipolar cells (193), which also exhibit sustained release of neurotransmitter driven by graded changes in membrane potential. Information on the molecular substrates of the ribbon has been obtained from studies of both retinal and auditory receptor cells, although it should be noted that the retinal and auditory synapses are not functionally identical. They differ markedly in their kinetics, with the auditory synapse handling fast signals and the retinal pathway transmitting slow ones. The main structural components of the ribbon are ribeye/CtBP2 (269) and two large scaffolding proteins, piccolo and bassoon (63). Bassoon is thought to moor the ribbon at the release site (143) and, in the *bassoon* knockout, the ribbon is no longer retained at the active zone, with the result that fast exocytosis is impaired. The exact contribution of the ribbon components is not fully understood: in the retina a possible role of ribeye and bassoon may be to organize the voltage-dependent Ca^{2+} channels to the active zone (85). Ribeye also makes up most of the synaptic ribbon density in fish neuromast hair cells, and there it is necessary for colocalization of Ca^{2+} channels and synaptic ribbons (174). A further difference between the IHC synapse and other synapses is the absence of the usual SNARE proteins and priming factors of the Munc13 family (293), as well as the Ca^{2+} sensor, synaptotagmin (17, 213, 264, 293). What replaces the SNARE proteins is unknown, but instead of synaptotagmin, another Ca^{2+} binding protein, otoferlin, is present (257, 263); however, much disagreement exists about which step or steps in the fusion process otoferlin is involved with or regulates (225, 226).

As with other stages in auditory transduction, mechanistic insights have been derived from study of mutations that cause deafness due to defective transmission at the hair cell synapse. Mutations in the *OTOF* gene cause nonsyndromic human deafness, DFNB9 (315), and otoferlin knockout mice are profoundly deaf. In such knockout mice, exocytosis in IHCs is almost totally abolished, despite a normal Ca^{2+} current and ribbon appearance (257). While these results establish otoferlin as being necessary for synaptic transmission, its exact role has been more difficult to define. Synaptotagmin, the Ca^{2+} sensor at many other synapses, possesses two C2 domains, C2A and C2B, which are thought to be Ca^{2+} and membrane-binding sites and to act in combination with SNARE proteins

to initiate exocytosis. In contrast, otoferlin is a much larger protein with six C2 domains, C2A to C2F, at least five of which bind Ca^{2+} with high affinity. Based on the distribution of point mutations, the C2C and C2F domains are probably the most important (128,221,226). A missense mutation of the C2F domain in the *pachanga* mutant showed reduced exocytosis and slowed priming of vesicles in the readily releasable pool, implying otoferlin may underlie rapid replenishment of vesicles as well as fusion (225, 293). A mutation in the C2C domain, I515T, diminished otoferlin levels in the plasma membrane, and exocytosis during prolonged stimulation was strongly reduced, again indicating that the protein is critical for the reformation of fusion-competent synaptic vesicles (281). Because of the requirement for rapid and sustained neurotransmitter release at the IHC ribbon synapse, replenishment of the pool of readily releasable vesicles is probably a rate-limiting step. Another mutation causing defective IHC synaptic transmission occurs in the gene for the vesicular glutamate transporter (VGLUT3), a protein required for uptake of the glutamate into the IHC synaptic vesicles. Mutation of its gene, *SLC17A8*, causes nonsyndromic human deafness, DFNA25, and deafness in mice (258, 273).

Voltage-dependent calcium channel

At the IHC synapse, Ca^{2+} enters via the Cav1.3 L-type voltage-dependent Ca^{2+} channel and is responsible for triggering exocytosis. The Cav1.3 isoform has a restricted pattern of expression distinct from other isoforms employed in most central synapses (233). Central synapses almost never use L-type Ca^{2+} channels, and N-type and P-type Ca^{2+} channels are more common. In the IHC, Ca^{2+} channels are constructed from the Cav1.3 pore-forming subunit, along with the Cavβ2 auxiliary subunit (209). The channels are clustered in the plasma membrane beneath the ribbon opposite the postsynaptic density. When opened by depolarization, the Ca^{2+} channel is thought to generate a cloud of cytoplasmic Ca^{2+} around the docked vesicles of the readily releasable pool. In Cav1.3 knockouts, exocytosis was minimal when evoked by IHC depolarization, but it was more robust when induced by elevating cytoplasmic Ca^{2+} by photolysis of caged Ca^{2+} (29). The result demonstrates a defect in Ca^{2+} influx, rather than in the subsequent release apparatus.

Synaptic vesicle release from adult IHCs is thought to be triggered by a restricted domain of cytoplasmic Ca^{2+}. This has been referred to as a Ca^{2+} nanodomain and has been proposed to originate from influx via a single Ca^{2+} channel (224, 307), though alternatives involving multiple channels have been suggested, and are more likely. One such mechanism might arise because of clustering of Ca^{2+} channels and their synchronized opening on depolarization (106). Tight coupling between Ca^{2+} influx and exocytosis has been supported by the lack of effect of fast calcium buffers on release. The faster a buffer's Ca^{2+} binding rate, the smaller the distance from the source over which it can buffer (207). Thus, intracellular perfusion with even a fast buffer like BAPTA has minimal effect on exocytosis, and multivesicular release persists in 10 mM intracellular BAPTA (103, 224). This suggest that each Ca^{2+} channel is no more than ~20 nm from the Ca^{2+} sensor and only a few channels may interact with a vesicle. However, BAPTA could also reduce the capacity of multiple Ca^{2+} sources to sum, thereby reducing a domain of Ca^{2+} under the ribbon. This was previously demonstrated from the effects of BAPTA on the gating of Ca^{2+}-activated K^+ (BK) channels in frog hair cells. Mirroring exocytosis, BK channels are activated by cytoplasmic Ca^{2+} generated by influx through a submicrometer array of about 100 channels near the ribbon (252, 253). The ribbon restricts the available volume beneath the presynaptic membrane containing the Ca^{2+} channel cluster, and in this space, a mobile calcium buffer, even 10 mmol/L BAPTA, quickly becomes saturated with Ca^{2+} influx. The physiological buffers in IHCs will be even less effective (110, 129). The presynaptic geometry around the ribbon permits large and fast elevation of cytoplasmic Ca^{2+} in the restricted volume, achieving free Ca^{2+} concentrations of tens of micromolar (252, 289), which can trigger multivesicular release, the synchronized release of an array of docked vesicles (106). The spatial arrangement also ensures that intracellular Ca^{2+} quickly returns to its resting level after the channels have closed, and so enables high frequency phase locking (252).

These properties apply to the mature synapse, which in adult rodents differs from that in neonates prior to the onset of hearing. At the earlier developmental stage, coupling is less tight, and is controlled by Ca^{2+} microdomains encompassing multiple channels spread over a larger area, with the Ca^{2+} cooperativity for transmitter release being approximately fourth power (131, 307); that is, transmitter release increases in proportion to the fourth power of the Ca^{2+} influx. The developmental switch from cooperative (fourth power) to linear (first power) release has been attributed to a topographic reorganization of the Ca^{2+} channels, from a more distributed array of channels in the neonate to their concentration under the active zone in the adult (307). The timing of the switch is concurrent with a transformation in the IHC voltage signals, from all-or-nothing action potentials to graded receptor potentials. In the neonate, IHCs exhibit Ca^{2+}-dependent action potentials that drive spontaneous firing in the auditory nerve; these signals may contribute to the refinement and maintenance of tonotopic maps in the auditory brainstem (288, 296). The action potentials disappear in the adult, when sound-evoked receptor potentials that are graded with stimulus intensity first appear (186). The linear Ca^{2+} dependence of exocytosis in mature IHCs enables the synapse to be sensitive to low-level stimuli and ensures that the amplitude of the receptor potentials is faithfully relayed to the nerve over a wide dynamic range.

Signaling of sound intensity over a wide dynamic range may also be assisted by the differential sensitivities of the synapses, with those with high sensitivity being located on the pillar side of the IHC and those with low sensitivity on the modiolar side (Fig. 15). While the origin of this heterogeneity

is still not fully established, several possibilities exist with differences originating on either the presynaptic or postsynaptic side. Immunolabeling of the postsynaptic membrane showed a higher density of GluA2/3 glutamate receptors on the pillar side of the IHC compared to the modiolar/basal zone, a variation that would be consistent with the proposed difference in sensitivity (163). In addition, there were differences in the size of the synaptic ribbon, with the ribbons on modiolar side being larger and more elongated; however, the significance of this observation is obscure. Other work has suggested a presynaptic variation such that Cav1.3 Ca^{2+} channels on the pillar side may activate at more hyperpolarized potentials than those on the modiolar side, thereby allowing Ca^{2+} entry for weaker depolarization (217). At this stage, the origin of the heterogeneity in synaptic sensitivities and related spontaneous activities is not fully understood.

Hidden hearing loss

Exposure to loud sounds has been known for some time to cause hearing loss. For lower sound intensities, the loss can be transient with an elevation in acoustic threshold that gradually returns to normal over a week or so. However, with louder sounds, prolonged exposure, or both, hearing loss can become permanent. For example, noise exposure of 85 dBA for an 8-h working day is regarded as the safe limit for factory workers, but the recommended dosages become briefer with more intense sounds: 100 dBA at 15 min and 110 dBA at 1.5 min (National Institute for Occupational Safety and Health, 1998 (1). Permanent hearing loss has been attributed to hair cell damage and death, especially for OHCs (168); since these cells do not regenerate, no compensatory recovery of hearing can occur. However, it has been recently appreciated that even at moderate sound levels, causing only temporary threshold shifts and no apparent hair cell damage, there is loss of the afferent nerve terminals to the IHCs, which eventually results in degeneration of the cell body in the spiral ganglion (156, 164). Remarkably, this cellular destruction can occur without any obvious change in behavioral threshold curve, so it has been referred to as "hidden hearing loss." As already noted, each IHC is innervated by multiple (10-20) auditory nerve terminals, and 50 percent of these terminals can be lost without a change in the behavioral threshold (156, 164). Although a reduction in the number of afferent fibers per IHC has no effect on the behavioral audiogram, it has been suggested to diminish human auditory performance on more complex tasks such as speech discrimination in noise. Another unexpected observation was that the loss of terminals was largely restricted to the high-threshold fibers that have low spontaneous activity (90). The precise mechanism of the loss is like other aspects of this synapse—not fully understood. One explanation is that it may involve toxicity caused by excess release of glutamate neurotransmitter, producing swelling and degeneration of the nerve terminals (164). This toxic effect may be larger on high-threshold fibers originating from smaller terminals with fewer mitochondria.

Cochlear efferent innervation

Besides the afferent innervation to the IHCs, there is also a cochlear efferent innervation, which originates principally from the contralateral superior olive and travels in the crossed olivocochlear bundle [for review see reference (107)]. In the adult mammal, medial olivocochlear fibers make large cholinergic synapses on OHCs, whereas lateral olivocochlear fibers terminate on the radial dendrites of the cochlear afferent neurons. Electrical stimulation of the crossed medial olivocochlear bundle in the floor of the fourth ventricle in intact animals produces desensitization of IHC receptor potentials (30) and 10 to 25 dB elevation of auditory nerve fiber thresholds (304), with the effects being mainly restricted to frequencies around the CF (107). Thus, the efferent action is manifest as a decreased frequency tuning of the auditory nerve fibers. Since the efferent fibers innervate the OHCs, these observations support the idea that the main effect is a decrease in the cochlear amplification mediated by the OHCs.

The mechanism of this cholinergic synapse is unusual [reviewed (88)]. It exhibits features of a neuronal acetylcholine receptor (nAChR), being linked to opening of a nonselective cation channel, and blocked by curare and α-bungarotoxin. However, the action of acetylcholine is inhibitory because of secondary activation of Ca^{2+}-dependent K^+ channels. The nAChR channels contain α9 and α10 nAChR subunits (72), rendering them very permeable to Ca^{2+}. When open, they promote Ca^{2+} influx, and the increase in cytoplasmic Ca^{2+} activates nearby SK2 and BK Ca^{2+}-dependent K^+ channels (149, 177, 303). A distinctive ultrastructural feature of the synapse is the submembranous cisterna adjacent to the OHC membrane opposite the presynaptic terminal. This cisterna, by analogy with the sarcoplasmic reticulum of muscle fibers, is thought to be a compartment for uptake and possible re-release of Ca^{2+} to buffer or augment the Ca^{2+} that has entered via the AChR channels (88). It presumably also confines the Ca^{2+} concentration increase to a small region of the cell around the synapse. As with neuronal inhibitory synapses, the mechanism of efferent inhibition may be the combined consequences of the change in membrane conductance and hyperpolarization. The increase in membrane conductance is expected to reduce the amplitude of the receptor potential; the hyperpolarization toward the K^+ equilibrium potential will shift the membrane potential away from that for optimal activation of prestin, approximately −50 mV. Besides these two established actions of an inhibitory neurotransmitter, there have been suggestions that electromotility in OHCs is also compromised by the ACh-induced increase in cytoplasmic Ca^{2+} that may alter the axial stiffness of the OHC (58, 87).

While the extent of efferent inhibition is only modest *in vivo*, its action on OHCs is sufficient to protect against noise-induced loss of cochlear neurons, the neuropathy underlying hidden hearing loss after moderate to high sound exposures (178). In those experiments, the site of action was localized by ablating the efferent innervation to either the OHCs

or the IHC afferents; the evoked neuropathy was largely confined to the OHCs, consistent with the role of these hair cells in cochlear amplification.

Conclusion

Understanding auditory transduction has required tackling several unusual physiological processes embodied in the mammalian cochlea. These processes involve the stria vascularis, a K^+ secretory epithelium that facilitates transduction and is able to develop 100 mV across its multicellular layers; the hair cell, a sensory neuron possessing a mechanically sensitive apparatus that can detect nanometer displacements on a microsecond time scale; and the OHC, which embodies a piezoelectric motor that displays electromotility at over 50 kHz without directly utilizing ATP. The assembly of cells in the cochlear partition, along with the basilar membrane, deconstructs incident sound stimuli into their frequency components. This process signals the respective amplitudes of the frequency components to the brain via synapses onto the auditory nerve of differential acoustic sensitivity. Investigating the underlying mechanisms has been hindered because the entire apparatus is encased in a bony shell and is very sensitive to mechanical and metabolic insults. Moreover, the experiments have necessitated acquiring techniques that can measure motion at a submicroscopic level. Nonetheless, substantial progress has occurred in all areas over the last 20 years. While the fundamental behavior of the cochlea as a spectrum analyzer has been known since the work of von Békésy, new discoveries about the molecular complexities of the hair bundle, an MET channel assembly likely to be distinct from the many mechanoreceptors elsewhere in the body, and a cochlear amplifier, which underlies sharp frequency selectivity and is based on the unique motor protein prestin, have been significant. In each area, advances have been propelled by exploration of genetic mutations, but important questions remain:

(i) What is the molecular makeup of the MET channel complex, and how does its composition enable the mechanical sensitivity and gating speed of the channel? Detailed knowledge of the channel structure may firmly establish the mechanism and role of Ca^{2+} in fast channel adaptation. A crucial aspect of the hair bundle is the staircase in stereociliary heights that confers directional sensitivity. Does development and preservation of the stereociliary staircase depend on operation of the MET channel?

(ii) Although prestin was cloned some time ago (320), its conformation, including the number of transmembrane domains, is still not firmly established. What is the origin of its voltage dependence and the structural rearrangement for expanding its area in the membrane, and how does this molecular motion affect OHC mechanics? Also, what part do chloride ions play in the activation of prestin by depolarization?

(iii) What are the cellular interactions in the organ of Corti consequent on mechanical stimulation and OHC contraction? Is the tunnel of Corti rigid due to buttressing by the pillar cells, and how do the Deiters' cells change shape? What are the magnitudes and phases of the cellular interactions within the organ of Corti, and importantly how do these interactions dictate mechanical feedback and ensure cochlear amplification? Since the stiffness of the basilar membrane is larger than the reticular lamina at the cochlear base but less than at the apex, how does deformation of the organ of Corti vary with the cochlear location?

(iv) There are multiple outstanding questions about the operation of the IHC synapse. What is the role of the ribbon, and why is otoferlin essential for performance? What is the source of the heterogeneity in synaptic sensitivities and spontaneous rates and is it presynaptic or postsynaptic? One of the most intriguing and clinically significant problems is the origin of the neuropathy associated with hidden hearing loss.

Despite substantial recent progress, many avenues remain for exploration in the physiology of the mammalian cochlea.

Acknowledgements

Work in the author's laboratory was funded by grant RO1 DC1362 from the National Institute on Deafness and Other Communication Disorders. I thank Maryline Beurg, Jong-Hoon Nam, Tony Ricci, Cyndie Chow, and Meyer Jackson for discussions.

References

1. Occupational Noise Exposure Cincinnati, OH: DHHS (NIOSH) Publication No. 98–126, 1998, p. 2-3.
2. Ahmed ZM, Goodyear R, Riazuddin S, Lagziel A, Legan PK, Behra M, Burgess SM, Lilley KS, Wilcox ER, Riazuddin S, Griffith AJ, Frolenkov GI, Belyantseva IA, Richardson GP, Friedman TB. The tip-link antigen, a protein associated with the transduction complex of sensory hair cells, is protocadherin-15. *J Neurosci* 26: 7022-7034, 2006.
3. Akinpelu OV, Peleva E, Funnell WR, Daniel SJ. Otoacoustic emissions in newborn hearing screening: A systematic review of the effects of different protocols on test outcomes. *Int J Pediatr Otorhinolaryngol* 78: 711-717, 2014.
4. Andrade LR, Salles FT, Grati M, Manor U, Kachar B. Tectorins crosslink type II collagen fibrils and connect the tectorial membrane to the spiral limbus. *J Struct Biol* 194: 139-146, 2016.
5. Art JJ, Fettiplace R. Variation of membrane properties in hair cells isolated from the turtle cochlea. *J Physiol* 385: 207-242, 1987.
6. Ashmore J. Cochlear outer hair cell motility. *Physiol Rev* 88: 173-210, 2008.
7. Ashmore JF. A fast motile response in guinea-pig outer hair cells: The cellular basis of the cochlear amplifier. *J Physiol* 388: 323-347, 1987.
8. Assad JA, Hacohen N, Corey DP. Voltage dependence of adaptation and active bundle movement in bullfrog saccular hair cells. *Proc Natl Acad Sci U S A* 86: 2918-2922, 1989.
9. Assad JA, Shepherd GM, Corey DP. Tip-link integrity and mechanical transduction in vertebrate hair cells. *Neuron* 7: 985-994, 1991.
10. Atkinson PJ, Huarcaya Najarro E, Sayyid ZN, Cheng AG. Sensory hair cell development and regeneration: Similarities and differences. *Development* 142: 1561-1571, 2015.

11. Bae C, Sachs F, Gottlieb PA. The mechanosensitive ion channel Piezo1 is inhibited by the peptide GsMTx4. *Biochemistry* 50: 6295-6300, 2011.
12. Barr-Gillespie PG. Assembly of hair bundles, an amazing problem for cell biology. *Mol Biol Cell* 26: 2727-2732, 2015.
13. Bekesy Gv. *Experiments in Hearing*. New York: McGraw-Hill, 1960.
14. Belyantseva IA, Boger ET, Naz S, Frolenkov GI, Sellers JR, Ahmed ZM, Griffith AJ, Friedman TB. Myosin-XVa is required for tip localization of whirlin and differential elongation of hair-cell stereocilia. *Nat Cell Biol* 7: 148-156, 2005.
15. Ben-Yosef T, Belyantseva IA, Saunders TL, Hughes ED, Kawamoto K, Van Itallie CM, Beyer LA, Halsey K, Gardner DJ, Wilcox ER, Rasmussen J, Anderson JM, Dolan DF, Forge A, Raphael Y, Camper SA, Friedman TB. Claudin 14 knockout mice, a model for autosomal recessive deafness DFNB29, are deaf due to cochlear hair cell degeneration. *Hum Mol Genet* 12: 2049-2061, 2003.
16. Beurg M, Evans MG, Hackney CM, Fettiplace R. A large-conductance calcium-selective mechanotransducer channel in mammalian cochlear hair cells. *J Neurosci* 26: 10992-11000, 2006.
17. Beurg M, Fettiplace R, Nam JH, Ricci AJ. Localization of inner hair cell mechanotransducer channels using high-speed calcium imaging. *Nat Neurosci* 12: 553-558, 2009.
18. Beurg M, Goldring AC, Fettiplace R. The effects of Tmc1 Beethoven mutation on mechanotransducer channel function in cochlear hair cells. *J Gen Physiol* 146: 233-243, 2015.
19. Beurg M, Kim KX, Fettiplace R. Conductance and block of hair-cell mechanotransducer channels in transmembrane channel-like protein mutants. *J Gen Physiol* 144: 55-69, 2014.
20. Beurg M, Nam JH, Chen Q, Fettiplace R. Calcium balance and mechanotransduction in rat cochlear hair cells. *J Neurophysiol* 104: 18-34, 2010.
21. Beurg M, Nam JH, Crawford A, Fettiplace R. The actions of calcium on hair bundle mechanics in mammalian cochlear hair cells. *Biophys J* 94: 2639-2653, 2008.
22. Beurg M, Tan X, Fettiplace R. A prestin motor in chicken auditory hair cells: Active force generation in a nonmammalian species. *Neuron* 79: 69-81, 2013.
23. Beurg M, Xiong W, Zhao B, Muller U, Fettiplace R. Subunit determination of the conductance of hair-cell mechanotransducer channels. *Proc Natl Acad Sci U S A* 112: 1589-1594, 2015.
24. Beutner D, Voets T, Neher E, Moser T. Calcium dependence of exocytosis and endocytosis at the cochlear inner hair cell afferent synapse. *Neuron* 29: 681-690, 2001.
25. Bohne BA, Carr CD. Morphometric analysis of hair cells in the chinchilla cochlea. *J Acoust Soc Am* 77: 153-158, 1985.
26. Borst JG, Soria van Hoeve J. The calyx of Held synapse: From model synapse to auditory relay. *Annu Rev Physiol* 74: 199-224, 2012.
27. Bosher SK. The nature of the negative endocochlear potentials produced by anoxia and ethacrynic acid in the rat and guinea-pig. *J Physiol* 293: 329-345, 1979.
28. Bosher SK, Warren RL. Very low calcium content of cochlear endolymph, an extracellular fluid. *Nature* 273: 377-378, 1978.
29. Brandt A, Striessnig J, Moser T. CaV1.3 channels are essential for development and presynaptic activity of cochlear inner hair cells. *J Neurosci* 23: 10832-10840, 2003.
30. Brown MC, Nuttall AL. Efferent control of cochlear inner hair cell responses in the guinea-pig. *J Physiol* 354: 625-646, 1984.
31. Brown MC, Nuttall AL, Masta RI, Lawrence M. Cochlear inner hair cells: Effects of transient asphyxia on intracellular potentials. *Hear Res* 9: 131-144, 1983.
32. Brownell WE, Bader CR, Bertrand D, de Ribaupierre Y. Evoked mechanical responses of isolated cochlear outer hair cells. *Science* 227: 194-196, 1985.
33. Chan DK, Hudspeth AJ. Ca2+ current-driven nonlinear amplification by the mammalian cochlea in vitro. *Nat Neurosci* 8: 149-155, 2005.
34. Chapman ER. How does synaptotagmin trigger neurotransmitter release? *Annu Rev Biochem* 77: 615-641, 2008.
35. Chapochnikov NM, Takago H, Huang CH, Pangrsic T, Khimich D, Neef J, Auge E, Gottfert F, Hell SW, Wichmann C, Wolf F, Moser T. Uniquantal release through a dynamic fusion pore is a candidate mechanism of hair cell exocytosis. *Neuron* 83: 1389-1403, 2014.
36. Chatzigeorgiou M, Bang S, Hwang SW, Schafer WR. tmc-1 encodes a sodium-sensitive channel required for salt chemosensation in C. elegans. *Nature* 494: 95-99, 2013.
37. Cheatham MA, Goodyear RJ, Homma K, Legan PK, Korchagina J, Naskar S, Siegel JH, Dallos P, Zheng J, Richardson GP. Loss of the tectorial membrane protein CEACAM16 enhances spontaneous, stimulus-frequency, and transiently evoked otoacoustic emissions. *J Neurosci* 34: 10325-10338, 2014.
38. Chen F, Zha D, Fridberger A, Zheng J, Choudhury N, Jacques SL, Wang RK, Shi X, Nuttall AL. A differentially amplified motion in the ear for near-threshold sound detection. *Nat Neurosci* 14: 770-774, 2011.
39. Chen Q, Mahendrasingam S, Tickle JA, Hackney CM, Furness DN, Fettiplace R. The development, distribution and density of the plasma membrane calcium ATPase 2 calcium pump in rat cochlear hair cells. *Eur J Neurosci* 36: 2302-2310, 2012.
40. Cheung EL, Corey DP. Ca2+ changes the force sensitivity of the hair-cell transduction channel. *Biophys J* 90: 124-139, 2006.
41. Clark GM. The multichannel cochlear implant for severe-to-profound hearing loss. *Nat Med* 19: 1236-1239, 2013.
42. Clark GM. The multi-channel cochlear implant: Multi-disciplinary development of electrical stimulation of the cochlea and the resulting clinical benefit. *Hear Res* 322: 4-13, 2015.
43. Cohen-Salmon M, Ott T, Michel V, Hardelin JP, Perfettini I, Eybalin M, Wu T, Marcus DC, Wangemann P, Willecke K, Petit C. Targeted ablation of connexin26 in the inner ear epithelial gap junction network causes hearing impairment and cell death. *Curr Biol* 12: 1106-1111, 2002.
44. Cooper NP. An improved heterodyne laser interferometer for use in studies of cochlear mechanics. *J Neurosci Methods* 88: 93-102, 1999.
45. Cooper NP, Rhode WS. Basilar membrane mechanics in the hook region of cat and guinea-pig cochleae: Sharp tuning and nonlinearity in the absence of baseline position shifts. *Hear Res* 63: 163-190, 1992.
46. Cooper NP, Rhode WS. Nonlinear mechanics at the apex of the guinea-pig cochlea. *Hear Res* 82: 225-243, 1995.
47. Corey DP, Hudspeth AJ. Kinetics of the receptor current in bullfrog saccular hair cells. *J Neurosci* 3: 962-976, 1983.
48. Corns LF, Johnson SL, Kros CJ, Marcotti W. Calcium entry into stereocilia drives adaptation of the mechanoelectrical transducer current of mammalian cochlear hair cells. *Proc Natl Acad Sci U S A* 111: 14918-14923, 2014.
49. Corns LF, Johnson SL, Kros CJ, Marcotti W. Tmc1 point mutation affects Ca2+ sensitivity and block by dihydrostreptomycin of the mechanoelectrical transducer current of mouse outer hair cells. *J Neurosci* 36: 336-349, 2016.
50. Coste B, Murthy SE, Mathur J, Schmidt M, Mechioukhi Y, Delmas P, Patapoutian A. Piezo1 ion channel pore properties are dictated by C-terminal region. *Nat Commun* 6: 7223, 2015.
51. Crawford AC, Evans MG, Fettiplace R. Activation and adaptation of transducer currents in turtle hair cells. *J Physiol* 419: 405-434, 1989.
52. Crawford AC, Evans MG, Fettiplace R. The actions of calcium on the mechano-electrical transducer current of turtle hair cells. *J Physiol* 434: 369-398, 1991.
53. Crawford AC, Fettiplace R. The frequency selectivity of auditory nerve fibres and hair cells in the cochlea of the turtle. *J Physiol* 306: 79-125, 1980.
54. Crawford AC, Fettiplace R. An electrical tuning mechanism in turtle cochlear hair cells. *J Physiol* 312: 377-412, 1981.
55. Crawford AC, Fettiplace R. The mechanical properties of ciliary bundles of turtle cochlear hair cells. *J Physiol* 364: 359-379, 1985.
56. Dallos P. Peripheral mechanisms of hearing. In: *Handbook of Physiology, The Nervous System, Sensory Processes*: American Physiological Society, pp. 595-637, 1984.
57. Dallos P. Response characteristics of mammalian cochlear hair cells. *J Neurosci* 5: 1591-1608, 1985.
58. Dallos P, He DZ, Lin X, Sziklai I, Mehta S, Evans BN. Acetylcholine, outer hair cell electromotility, and the cochlear amplifier. *J Neurosci* 17: 2212-2226, 1997.
59. Dallos P, Wu X, Cheatham MA, Gao J, Zheng J, Anderson CT, Jia S, Wang X, Cheng WH, Sengupta S, He DZ, Zuo J. Prestin-based outer hair cell motility is necessary for mammalian cochlear amplification. *Neuron* 58: 333-339, 2008.
60. Dannhof BJ, Roth B, Bruns V. Length of hair cells as a measure of frequency representation in the mammalian inner ear? *Naturwissenschaften* 78: 570-573, 1991.
61. Davis H. An active process in cochlear mechanics. *Hear Res* 9: 79-90, 1983.
62. Delprat B, Michel V, Goodyear R, Yamasaki Y, Michalski N, El-Amraoui A, Perfettini I, Legrain P, Richardson G, Hardelin JP, Petit C. Myosin XVa and whirlin, two deafness gene products required for hair bundle growth, are located at the stereocilia tips and interact directly. *Hum Mol Genet* 14: 401-410, 2005.
63. Dick O, Hack I, Altrock WD, Garner CC, Gundelfinger ED, Brandstatter JH. Localization of the presynaptic cytomatrix protein Piccolo at ribbon and conventional synapses in the rat retina: Comparison with Bassoon. *J Comp Neurol* 439: 224-234, 2001.
64. Dixon MJ, Gazzard J, Chaudhry SS, Sampson N, Schulte BA, Steel KP. Mutation of the Na-K-Cl co-transporter gene Slc12a2 results in deafness in mice. *Hum Mol Genet* 8: 1579-1584, 1999.
65. Doll JC, Peng AW, Ricci AJ, Pruitt BL. Faster than the speed of hearing: Nanomechanical force probes enable the electromechanical observation of cochlear hair cells. *Nano Lett* 12: 6107-6111, 2012.
66. Dong W, Cooper NP. An experimental study into the acousto-mechanical effects of invading the cochlea. *J R Soc Interface* 3: 561-571, 2006.
67. Dong W, Olson ES. Detection of cochlear amplification and its activation. *Biophys J* 105: 1067-1078, 2013.

68. Dumont RA, Lins U, Filoteo AG, Penniston JT, Kachar B, Gillespie PG. Plasma membrane Ca2+-ATPase isoform 2a is the PMCA of hair bundles. *J Neurosci* 21: 5066-5078, 2001.
69. Eatock RA. Adaptation in hair cells. *Annu Rev Neurosci* 23: 285-314, 2000.
70. Eatock RA, Corey DP, Hudspeth AJ. Adaptation of mechanoelectrical transduction in hair cells of the bullfrog's sacculus. *J Neurosci* 7: 2821-2836, 1987.
71. Ebrahim S, Avenarius MR, Grati M, Krey JF, Windsor AM, Sousa AD, Ballesteros A, Cui R, Millis BA, Salles FT, Baird MA, Davidson MW, Jones SM, Choi D, Dong L, Raval MH, Yengo CM, Barr-Gillespie PG, Kachar B. Stereocilia-staircase spacing is influenced by myosin III motors and their cargos espin-1 and espin-like. *Nat Commun* 7: 10833, 2016.
72. Elgoyhen AB, Katz E, Fuchs PA. The nicotinic receptor of cochlear hair cells: A possible pharmacotherapeutic target? *Biochem Pharmacol* 78: 712-719, 2009.
73. Emadi G, Richter CP, Dallos P. Stiffness of the gerbil basilar membrane: Radial and longitudinal variations. *J Neurophysiol* 91: 474-488, 2004.
74. Evans EF, Klinke R. The effects of intracochlear and systemic furosemide on the properties of single cochlear nerve fibres in the cat. *J Physiol* 331: 409-427, 1982.
75. Everett LA, Morsli H, Wu DK, Green ED. Expression pattern of the mouse ortholog of the Pendred's syndrome gene (Pds) suggests a key role for pendrin in the inner ear. *Proc Natl Acad Sci U S A* 96: 9727-9732, 1999.
76. Farris HE, LeBlanc CL, Goswami J, Ricci AJ. Probing the pore of the auditory hair cell mechanotransducer channel in turtle. *J Physiol* 558: 769-792, 2004.
77. Fay RR. *Hearing in Vertebrates: A Psychophysics Databook*. Winnetka, IL: Hill-Fay Associates, 1988.
78. Fettiplace R. Is TMC1 the hair cell mechanotransducer channel? *Biophys J* 111: 3-9, 2016.
79. Fettiplace R, Fuchs PA. Mechanisms of hair cell tuning. *Annu Rev Physiol* 61: 809-834, 1999.
80. Fettiplace R, Kim KX. The physiology of mechanoelectrical transduction channels in hearing. *Physiol Rev* 94: 951-986, 2014.
81. Fettiplace R, Ricci AJ. Mechanoelectrical transduction in auditory hair cells. In: *Vertebrate Hair Cells*, edited by Eatock RA, Fay RR and Popper AN. New York: Springer, pp. 154-203, 2006.
82. Fisher JA, Nin F, Reichenbach T, Uthaiah RC, Hudspeth AJ. The spatial pattern of cochlear amplification. *Neuron* 76: 989-997, 2012.
83. Flagella M, Clarke LL, Miller ML, Erway LC, Giannella RA, Andringa A, Gawenis LR, Kramer J, Duffy JJ, Doetschman T, Lorenz JN, Yamoah EN, Cardell EL, Shull GE. Mice lacking the basolateral Na-K-2Cl cotransporter have impaired epithelial chloride secretion and are profoundly deaf. *J Biol Chem* 274: 26946-26955, 1999.
84. Frank G, Hemmert W, Gummer AW. Limiting dynamics of high-frequency electromechanical transduction of outer hair cells. *Proc Natl Acad Sci U S A* 96: 4420-4425, 1999.
85. Frank T, Rutherford MA, Strenzke N, Neef A, Pangrsic T, Khimich D, Fejtova A, Gundelfinger ED, Liberman MC, Harke B, Bryan KE, Lee A, Egner A, Riedel D, Moser T. Bassoon and the synaptic ribbon organize Ca(2)+ channels and vesicles to add release sites and promote refilling. *Neuron* 68: 724-738, 2010.
86. Fridberger A, Tomo I, Ulfendahl M, Boutet de Monvel J. Imaging hair cell transduction at the speed of sound: dynamic behavior of mammalian stereocilia. *Proc Natl Acad Sci U S A* 103: 1918-1923, 2006.
87. Frolenkov GI. Regulation of electromotility in the cochlear outer hair cell. *J Physiol* 576: 43-48, 2006.
88. Fuchs PA. A 'calcium capacitor' shapes cholinergic inhibition of cochlear hair cells. *J Physiol* 592: 3393-3401, 2014.
89. Fuchs PA, Glowatzki E. Synaptic studies inform the functional diversity of cochlear afferents. *Hear Res* 330: 18-25, 2015.
90. Furman AC, Kujawa SG, Liberman MC. Noise-induced cochlear neuropathy is selective for fibers with low spontaneous rates. *J Neurophysiol* 110: 577-586, 2013.
91. Furness DN, Katori Y, Nirmal Kumar B, Hackney CM. The dimensions and structural attachments of tip links in mammalian cochlear hair cells and the effects of exposure to different levels of extracellular calcium. *Neuroscience* 154: 10-21, 2008.
92. Gale JE, Marcotti W, Kennedy HJ, Kros CJ, Richardson GP. FM1-43 dye behaves as a permeant blocker of the hair-cell mechanotransducer channel. *J Neurosci* 21: 7013-7025, 2001.
93. Geisler CD, Sang C. A cochlear model using feed-forward outer-hair-cell forces. *Hear Res* 86: 132-146, 1995.
94. Geleoc GS, Lennan GW, Richardson GP, Kros CJ. A quantitative comparison of mechanoelectrical transduction in vestibular and auditory hair cells of neonatal mice. *Proc Biol Sci* 264: 611-621, 1997.
95. Ghaffari R, Aranyosi AJ, Richardson GP, Freeman DM. Tectorial membrane travelling waves underlie abnormal hearing in Tectb mutant mice. *Nat Commun* 1: 96, 2010.
96. Gill SS, Salt AN. Quantitative differences in endolymphatic calcium and endocochlear potential between pigmented and albino guinea pigs. *Hear Res* 113: 191-197, 1997.
97. Gillespie PG, Cyr JL. Myosin-1c, the hair cell's adaptation motor. *Annu Rev Physiol* 66: 521-545, 2004.
98. Gleason MR, Nagiel A, Jamet S, Vologodskaia M, Lopez-Schier H, Hudspeth AJ. The transmembrane inner ear (Tmie) protein is essential for normal hearing and balance in the zebrafish. *Proc Natl Acad Sci U S A* 106: 21347-21352, 2009.
99. Glowatzki E, Fuchs PA. Transmitter release at the hair cell ribbon synapse. *Nat Neurosci* 5: 147-154, 2002.
100. Goodyear RJ, Marcotti W, Kros CJ, Richardson GP. Development and properties of stereociliary link types in hair cells of the mouse cochlea. *J Comp Neurol* 485: 75-85, 2005.
101. Gorbunov D, Sturlese M, Nies F, Kluge M, Bellanda M, Battistutta R, Oliver D. Molecular architecture and the structural basis for anion interaction in prestin and SLC26 transporters. *Nat Commun* 5: 3622, 2014.
102. Goutman JD. Transmitter release from cochlear hair cells is phase locked to cyclic stimuli of different intensities and frequencies. *J Neurosci* 32: 17025-17035a, 2012.
103. Goutman JD, Glowatzki E. Time course and calcium dependence of transmitter release at a single ribbon synapse. *Proc Natl Acad Sci U S A* 104: 16341-16346, 2007.
104. Gow A, Davies C, Southwood CM, Frolenkov G, Chrustowski M, Ng L, Yamauchi D, Marcus DC, Kachar B. Deafness in Claudin 11-null mice reveals the critical contribution of basal cell tight junctions to stria vascularis function. *J Neurosci* 24: 7051-7062, 2004.
105. Grati M, Kachar B. Myosin VIIa and sans localization at stereocilia upper tip-link density implicates these Usher syndrome proteins in mechanotransduction. *Proc Natl Acad Sci U S A* 108: 11476-11481, 2011.
106. Graydon CW, Cho S, Li GL, Kachar B, von Gersdorff H. Sharp Ca(2)(+) nanodomains beneath the ribbon promote highly synchronous multivesicular release at hair cell synapses. *J Neurosci* 31: 16637-16650, 2011.
107. Guinan JJ. Efferent Physiology. In: *The Cochlea*, edited by Dallos P, Popper AN and Fay RR. New York: Springer Verlag, pp. 435-502, 1996.
108. Gummer AW, Hemmert W, Zenner HP. Resonant tectorial membrane motion in the inner ear: Its crucial role in frequency tuning. *Proc Natl Acad Sci U S A* 93: 8727-8732, 1996.
109. Guo Y, Wang Y, Zhang W, Meltzer S, Zanini D, Yu Y, Li J, Cheng T, Guo Z, Wang Q, Jacobs JS, Sharma Y, Eberl DF, Gopfert MC, Jan LY, Jan YN, Wang Z. Transmembrane channel-like (tmc) gene regulates Drosophila larval locomotion. *Proc Natl Acad Sci U S A* 113: 7243-7248, 2016.
110. Hackney CM, Mahendrasingam S, Penn A, Fettiplace R. The concentrations of calcium buffering proteins in mammalian cochlear hair cells. *J Neurosci* 25: 7867-7875, 2005.
111. Hacohen N, Assad JA, Smith WJ, Corey DP. Regulation of tension on hair-cell transduction channels: Displacement and calcium dependence. *J Neurosci* 9: 3988-3997, 1989.
112. He DZ, Jia S, Dallos P. Mechanoelectrical transduction of adult outer hair cells studied in a gerbil hemicochlea. *Nature* 429: 766-770, 2004.
113. He DZ, Jia S, Sato T, Zuo J, Andrade LR, Riordan GP, Kachar B. Changes in plasma membrane structure and electromotile properties in prestin deficient outer hair cells. *Cytoskeleton (Hoboken)* 67: 43-55, 2010.
114. Hille B. *Ion Channels of Excitable Membranes* (3rd ed.). Sunderland, MA: Sinauer, 2001.
115. Holley MC, Ashmore JF. On the mechanism of a high-frequency force generator in outer hair cells isolated from the guinea pig cochlea. *Proc R Soc Lond B Biol Sci* 232: 413-429, 1988.
116. Holton T, Hudspeth AJ. The transduction channel of hair cells from the bull-frog characterized by noise analysis. *J Physiol* 375: 195-227, 1986.
117. Housley GD, Ashmore JF. Ionic currents of outer hair cells isolated from the guinea-pig cochlea. *J Physiol* 448: 73-98, 1992.
118. Howard J, Hudspeth AJ. Mechanical relaxation of the hair bundle mediates adaptation in mechanoelectrical transduction by the bullfrog's saccular hair cell. *Proc Natl Acad Sci U S A* 84: 3064-3068, 1987.
119. Howard J, Hudspeth AJ. Compliance of the hair bundle associated with gating of mechanoelectrical transduction channels in the bullfrog's saccular hair cell. *Neuron* 1: 189-199, 1988.
120. Hudspeth AJ. Integrating the active process of hair cells with cochlear function. *Nat Rev Neurosci* 15: 600-614, 2014.
121. Hudspeth AJ, Lewis RS. A model for electrical resonance and frequency tuning in saccular hair cells of the bull-frog, Rana catesbeiana. *J Physiol* 400: 275-297, 1988.
122. Huth ME, Ricci AJ, Cheng AG. Mechanisms of aminoglycoside ototoxicity and targets of hair cell protection. *Int J Otolaryngol* 2011: 937861, 2011.

123. Ikeda K, Kusakari J, Takasaka T, Saito Y. The Ca2+ activity of cochlear endolymph of the guinea pig and the effect of inhibitors. *Hear Res* 26: 117-125, 1987.
124. Iwasa KH, Adachi M. Force generation in the outer hair cell of the cochlea. *Biophys J* 73: 546-555, 1997.
125. Javel E. Shapes of cat auditory nerve fiber tuning curves. *Hear Res* 81: 167-188, 1994.
126. Jentsch TJ. Neuronal KCNQ potassium channels: Physiology and role in disease. *Nat Rev Neurosci* 1: 21-30, 2000.
127. Jia S, Dallos P, He DZ. Mechanoelectric transduction of adult inner hair cells. *J Neurosci* 27: 1006-1014, 2007.
128. Johnson CP, Chapman ER. Otoferlin is a calcium sensor that directly regulates SNARE-mediated membrane fusion. *J Cell Biol* 191: 187-197, 2010.
129. Johnson SL, Beurg M, Marcotti W, Fettiplace R. Prestin-driven cochlear amplification is not limited by the outer hair cell membrane time constant. *Neuron* 70: 1143-1154, 2011.
130. Johnson SL, Kennedy HJ, Holley MC, Fettiplace R, Marcotti W. The resting transducer current drives spontaneous activity in prehearing mammalian cochlear inner hair cells. *J Neurosci* 32: 10479-10483, 2012.
131. Johnson SL, Marcotti W, Kros CJ. Increase in efficiency and reduction in Ca2 +dependence of exocytosis during development of mouse inner hair cells. *J Physiol* 563: 177-191, 2005.
132. Jones GP, Elliott SJ, Russell IJ, Lukashkin AN. Modified protein expression in the tectorial membrane of the cochlea reveals roles for the striated sheet matrix. *Biophys J* 108: 203-210, 2015.
133. Joris P, Yin TC. A matter of time: Internal delays in binaural processing. *Trends Neurosci* 30: 70-78, 2007.
134. Karavitaki KD, Mountain DC. Imaging electrically evoked micromechanical motion within the organ of corti of the excised gerbil cochlea. *Biophys J* 92: 3294-3316, 2007.
135. Kawashima Y, Geleoc GS, Kurima K, Labay V, Lelli A, Asai Y, Makishima T, Wu DK, Della Santina CC, Holt JR, Griffith AJ. Mechanotransduction in mouse inner ear hair cells requires transmembrane channel-like genes. *J Clin Invest* 121: 4796-4809, 2011.
136. Kazmierczak P, Sakaguchi H, Tokita J, Wilson-Kubalek EM, Milligan RA, Muller U, Kachar B. Cadherin 23 and protocadherin 15 interact to form tip-link filaments in sensory hair cells. *Nature* 449: 87-91, 2007.
137. Keen EC, Hudspeth AJ. Transfer characteristics of the hair cell's afferent synapse. *Proc Natl Acad Sci U S A* 103: 5537-5542, 2006.
138. Kemp DT. Otoacoustic emissions, their origin in cochlear function, and use. *Br Med Bull* 63: 223-241, 2002.
139. Kennedy HJ, Crawford AC, Fettiplace R. Force generation by mammalian hair bundles supports a role in cochlear amplification. *Nature* 433: 880-883, 2005.
140. Kennedy HJ, Evans MG, Crawford AC, Fettiplace R. Fast adaptation of mechanoelectrical transducer channels in mammalian cochlear hair cells. *Nat Neurosci* 6: 832-836, 2003.
141. Kennedy HJ, Evans MG, Crawford AC, Fettiplace R. Depolarization of cochlear outer hair cells evokes active hair bundle motion by two mechanisms. *J Neurosci* 26: 2757-2766, 2006.
142. Kharkovets T, Dedek K, Maier H, Schweizer M, Khimich D, Nouvian R, Vardanyan V, Leuwer R, Moser T, Jentsch TJ. Mice with altered KCNQ4 K+ channels implicate sensory outer hair cells in human progressive deafness. *Embo j* 25: 642-652, 2006.
143. Khimich D, Nouvian R, Pujol R, Tom Dieck S, Egner A, Gundelfinger ED, Moser T. Hair cell synaptic ribbons are essential for synchronous auditory signalling. *Nature* 434: 889-894, 2005.
144. Kiang NYS. Peripheral neural processing of auditory information. In: *Handbook of Physiology, The Nervous System, Sensory Processes*: American Physiological Society, pp. 639-674, 1984.
145. Kim KX, Beurg M, Hackney CM, Furness DN, Mahendrasingam S, Fettiplace R. The role of transmembrane channel-like proteins in the operation of hair cell mechanotransducer channels. *J Gen Physiol* 142: 493-505, 2013.
146. Kim KX, Fettiplace R. Developmental changes in the cochlear hair cell mechanotransducer channel and their regulation by transmembrane channel-like proteins. *J Gen Physiol* 141: 141-148, 2013.
147. Kitajiri S, Miyamoto T, Mineharu A, Sonoda N, Furuse K, Hata M, Sasaki H, Mori Y, Kubota T, Ito J, Furuse M, Tsukita S. Compartmentalization established by claudin-11-based tight junctions in stria vascularis is required for hearing through generation of endocochlear potential. *J Cell Sci* 117: 5087-5096, 2004.
148. Kitajiri S, Sakamoto T, Belyantseva IA, Goodyear RJ, Stepanyan R, Fujiwara I, Bird JE, Riazuddin S, Riazuddin S, Ahmed ZM, Hinshaw JE, Sellers J, Bartles JR, Hammer JA, III, Richardson GP, Griffith AJ, Frolenkov GI, Friedman TB. Actin-bundling protein TRIOBP forms resilient rootlets of hair cell stereocilia essential for hearing. *Cell* 141: 786-798, 2010.
149. Kong JH, Adelman JP, Fuchs PA. Expression of the SK2 calcium-activated potassium channel is required for cholinergic function in mouse cochlear hair cells. *J Physiol* 586: 5471-5485, 2008.
150. Kozel PJ, Friedman RA, Erway LC, Yamoah EN, Liu LH, Riddle T, Duffy JJ, Doetschman T, Miller ML, Cardell EL, Shull GE. Balance and hearing deficits in mice with a null mutation in the gene encoding plasma membrane Ca2+-ATPase isoform 2. *J Biol Chem* 273: 18693-18696, 1998.
151. Kozlov AS, Risler T, Hudspeth AJ. Coherent motion of stereocilia assures the concerted gating of hair-cell transduction channels. *Nat Neurosci* 10: 87-92, 2007.
152. Kros CJ. How to build an inner hair cell: Challenges for regeneration. *Hear Res* 227: 3-10, 2007.
153. Kros CJ, Crawford AC. Potassium currents in inner hair cells isolated from the guinea-pig cochlea. *J Physiol* 421: 263-291, 1990.
154. Kros CJ, Marcotti W, van Netten SM, Self TJ, Libby RT, Brown SD, Richardson GP, Steel KP. Reduced climbing and increased slipping adaptation in cochlear hair cells of mice with Myo7a mutations. *Nat Neurosci* 5: 41-47, 2002.
155. Kros CJ, Rusch A, Richardson GP. Mechano-electrical transducer currents in hair cells of the cultured neonatal mouse cochlea. *Proc Biol Sci* 249: 185-193, 1992.
156. Kujawa SG, Liberman MC. Adding insult to injury: Cochlear nerve degeneration after "temporary" noise-induced hearing loss. *J Neurosci* 29: 14077-14085, 2009.
157. Kurima K, Ebrahim S, Pan B, Sedlacek M, Sengupta P, Millis BA, Cui R, Nakanishi H, Fujikawa T, Kawashima Y, Choi BY, Monahan K, Holt JR, Griffith AJ, Kachar B. TMC1 and TMC2 localize at the site of mechanotransduction in mammalian inner ear hair cell stereocilia. *Cell Rep* 12: 1606-1617, 2015.
158. Kurima K, Peters LM, Yang Y, Riazuddin S, Ahmed ZM, Naz S, Arnaud D, Drury S, Mo J, Makishima T, Ghosh M, Menon PS, Deshmukh D, Oddoux C, Ostrer H, Khan S, Riazuddin S, Deininger PL, Hampton LL, Sullivan SL, Battey JF, Jr., Keats BJ, Wilcox ER, Friedman TB, Griffith AJ. Dominant and recessive deafness caused by mutations of a novel gene, TMC1, required for cochlear hair-cell function. *Nat Genet* 30: 277-284, 2002.
159. Labay V, Weichert RM, Makishima T, Griffith AJ. Topology of transmembrane channel-like gene 1 protein. *Biochemistry* 49: 8592-8598, 2010.
160. Lee HY, Raphael PD, Park J, Ellerbee AK, Applegate BE, Oghalai JS. Noninvasive in vivo imaging reveals differences between tectorial membrane and basilar membrane traveling waves in the mouse cochlea. *Proc Natl Acad Sci U S A* 112: 3128-3133, 2015.
161. Legan PK, Lukashkina VA, Goodyear RJ, Kossi M, Russell IJ, Richardson GP. A targeted deletion in alpha-tectorin reveals that the tectorial membrane is required for the gain and timing of cochlear feedback. *Neuron* 28: 273-285, 2000.
162. Li GL, Keen E, Andor-Ardo D, Hudspeth AJ, von Gersdorff H. The unitary event underlying multiquantal EPSCs at a hair cell's ribbon synapse. *J Neurosci* 29: 7558-7568, 2009.
163. Liberman LD, Wang H, Liberman MC. Opposing gradients of ribbon size and AMPA receptor expression underlie sensitivity differences among cochlear-nerve/hair-cell synapses. *J Neurosci* 31: 801-808, 2011.
164. Liberman MC. Noise-induced hearing loss: Permanent versus temporary threshold shifts and the effects of hair cell versus neuronal degeneration. *Adv Exp Med Biol* 875: 1-7, 2016.
165. Liberman MC. Auditory-nerve response from cats raised in a low-noise chamber. *J Acoust Soc Am* 63: 442-455, 1978.
166. Liberman MC. Morphological differences among radial afferent fibers in the cat cochlea: An electron-microscopic study of serial sections. *Hear Res* 3: 45-63, 1980.
167. Liberman MC. The cochlear frequency map for the cat: Labeling auditory-nerve fibers of known characteristic frequency. *J Acoust Soc Am* 72: 1441-1449, 1982.
168. Liberman MC, Dodds LW. Single-neuron labeling and chronic cochlear pathology. III. Stereocilia damage and alterations of threshold tuning curves. *Hear Res* 16: 55-74, 1984.
169. Liberman MC, Gao J, He DZ, Wu X, Jia S, Zuo J. Prestin is required for electromotility of the outer hair cell and for the cochlear amplifier. *Nature* 419: 300-304, 2002.
170. Lim DJ. Functional structure of the organ of Corti: A review. *Hear Res* 22: 117-146, 1986.
171. Liu Y, Gracewski SM, Nam JH. Consequences of location-dependent organ of corti micro-mechanics. *PLoS One* 10: e0133284, 2015.
172. Liu YP, Zhao HB. Cellular characterization of Connexin26 and Connnexin30 expression in the cochlear lateral wall. *Cell Tissue Res* 333: 395-403, 2008.
173. Longo-Guess CM, Gagnon LH, Cook SA, Wu J, Zheng QY, Johnson KR. A missense mutation in the previously undescribed gene Tmhs underlies deafness in hurry-scurry (hscy) mice. *Proc Natl Acad Sci U S A* 102: 7894-7899, 2005.
174. Lv C, Stewart WJ, Akanyeti O, Frederick C, Zhu J, Santos-Sacchi J, Sheets L, Liao JC, Zenisek D. Synaptic ribbons require ribeye for

electron density, proper synaptic localization, and recruitment of calcium channels. *Cell Rep* 15: 2784-2795, 2016.
175. Maeda R, Kindt KS, Mo W, Morgan CP, Erickson T, Zhao H, Clemens-Grisham R, Barr-Gillespie PG, Nicolson T. Tip-link protein protocadherin 15 interacts with transmembrane channel-like proteins TMC1 and TMC2. *Proc Natl Acad Sci U S A* 111: 12907-12912, 2014.
176. Mahendrasingam S, Beurg M, Fettiplace R, Hackney CM. The ultrastructural distribution of prestin in outer hair cells: A post-embedding immunogold investigation of low-frequency and high-frequency regions of the rat cochlea. *Eur J Neurosci* 31: 1595-1605, 2010.
177. Maison SF, Pyott SJ, Meredith AL, Liberman MC. Olivocochlear suppression of outer hair cells in vivo: Evidence for combined action of BK and SK2 channels throughout the cochlea. *J Neurophysiol* 109: 1525-1534, 2013.
178. Maison SF, Usubuchi H, Liberman MC. Efferent feedback minimizes cochlear neuropathy from moderate noise exposure. *J Neurosci* 33: 5542-5552, 2013.
179. Mammano F. Ca2+ homeostasis defects and hereditary hearing loss. *Biofactors* 37: 182-188, 2011.
180. Mammano F, Ashmore JF. Differential expression of outer hair cell potassium currents in the isolated cochlea of the guinea-pig. *J Physiol* 496(Pt 3): 639-646, 1996.
181. Mammano F, Ashmore JF. Reverse transduction measured in the isolated cochlea by laser Michelson interferometry. *Nature* 365: 838-841, 1993.
182. Manor U, Disanza A, Grati M, Andrade L, Lin H, Di Fiore PP, Scita G, Kachar B. Regulation of stereocilia length by myosin XVa and whirlin depends on the actin-regulatory protein Eps8. *Curr Biol* 21: 167-172, 2011.
183. Marcotti W, Corns LF, Goodyear RJ, Rzadzinska AK, Avraham KB, Steel KP, Richardson GP, Kros CJ. The acquisition of mechano-electrical transducer current adaptation in auditory hair cells requires myosin VI. *J Physiol* 594: 3667-3681, 2016.
184. Marcotti W, Johnson SL, Holley MC, Kros CJ. Developmental changes in the expression of potassium currents of embryonic, neonatal and mature mouse inner hair cells. *J Physiol* 548: 383-400, 2003.
185. Marcotti W, Johnson SL, Kros CJ. Effects of intracellular stores and extracellular Ca(2+) on Ca(2+)-activated K(+) currents in mature mouse inner hair cells. *J Physiol* 557: 613-633, 2004.
186. Marcotti W, Johnson SL, Rusch A, Kros CJ. Sodium and calcium currents shape action potentials in immature mouse inner hair cells. *J Physiol* 552: 743-761, 2003.
187. Marcotti W, Kros CJ. Developmental expression of the potassium current IK,n contributes to maturation of mouse outer hair cells. *J Physiol* 520(Pt 3): 653-660, 1999.
188. Marcotti W, van Netten SM, Kros CJ. The aminoglycoside antibiotic dihydrostreptomycin rapidly enters mouse outer hair cells through the mechano-electrical transducer channels. *J Physiol* 567: 505-521, 2005.
189. Marcus DC, Wu T, Wangemann P, Kofuji P. KCNJ10 (Kir4.1) potassium channel knockout abolishes endocochlear potential. *Am J Physiol Cell Physiol* 282: C403-407, 2002.
190. Markin VS, Hudspeth AJ. Gating-spring models of mechanoelectrical transduction by hair cells of the internal ear. *Annu Rev Biophys Biomol Struct* 24: 59-83, 1995.
191. Martin P, Bozovic D, Choe Y, Hudspeth AJ. Spontaneous oscillation by hair bundles of the bullfrog's sacculus. *J Neurosci* 23: 4533-4548, 2003.
192. Martin P, Hudspeth AJ. Active hair-bundle movements can amplify a hair cell's response to oscillatory mechanical stimuli. *Proc Natl Acad Sci U S A* 96: 14306-14311, 1999.
193. Matthews G, Fuchs P. The diverse roles of ribbon synapses in sensory neurotransmission. *Nat Rev Neurosci* 11: 812-822, 2010.
194. Mburu P, Mustapha M, Varela A, Weil D, El-Amraoui A, Holme RH, Rump A, Hardisty RE, Blanchard S, Coimbra RS, Perfettini I, Parkinson N, Mallon AM, Glenister P, Rogers MJ, Paige AJ, Moir L, Clay J, Rosenthal A, Liu XZ, Blanco G, Steel KP, Petit C, Brown SD. Defects in whirlin, a PDZ domain molecule involved in stereocilia elongation, cause deafness in the whirler mouse and families with DFNB31. *Nat Genet* 34: 421-428, 2003.
195. Meaud J, Grosh K. The effect of tectorial membrane and basilar membrane longitudinal coupling in cochlear mechanics. *J Acoust Soc Am* 127: 1411-1421, 2010.
196. Meaud J, Grosh K. Coupling active hair bundle mechanics, fast adaptation, and somatic motility in a cochlear model. *Biophys J* 100: 2576-2585, 2011.
197. Meyers JR, MacDonald RB, Duggan A, Lenzi D, Standaert DG, Corwin JT, Corey DP. Lighting up the senses: FM1-43 loading of sensory cells through nonselective ion channels. *J Neurosci* 23: 4054-4065, 2003.
198. Mistrik P, Mullaley C, Mammano F, Ashmore J. Three-dimensional current flow in a large-scale model of the cochlea and the mechanism of amplification of sound. *J R Soc Interface* 6: 279-291, 2009.
199. Mohrmann R, de Wit H, Connell E, Pinheiro PS, Leese C, Bruns D, Davletov B, Verhage M, Sorensen JB. Synaptotagmin interaction with SNAP-25 governs vesicle docking, priming, and fusion triggering. *J Neurosci* 33: 14417-14430, 2013.
200. Muller M. Developmental changes of frequency representation in the rat cochlea. *Hear Res* 56: 1-7, 1991.
201. Muller M. The cochlear place-frequency map of the adult and developing Mongolian gerbil. *Hear Res* 94: 148-156, 1996.
202. Muller M, von Hunerbein K, Hoidis S, Smolders JW. A physiological place-frequency map of the cochlea in the CBA/J mouse. *Hear Res* 202: 63-73, 2005.
203. Naidu RC, Mountain DC. Measurements of the stiffness map challenge a basic tenet of cochlear theories. *Hear Res* 124: 124-131, 1998.
204. Nam JH, Fettiplace R. Force transmission in the organ of Corti micromachine. *Biophys J* 98: 2813-2821, 2010.
205. Nam JH, Fettiplace R. Optimal electrical properties of outer hair cells ensure cochlear amplification. *PLoS One* 7: e50572, 2012.
206. Nam JH, Peng AW, Ricci AJ. Underestimated sensitivity of mammalian cochlear hair cells due to splay between stereociliary columns. *Biophys J* 108: 2633-2647, 2015.
207. Naraghi M, Neher E. Linearized buffered Ca2+ diffusion in microdomains and its implications for calculation of [Ca2+] at the mouth of a calcium channel. *J Neurosci* 17: 6961-6973, 1997.
208. Narayan SS, Temchin AN, Recio A, Ruggero MA. Frequency tuning of basilar membrane and auditory nerve fibers in the same cochleae. *Science* 282: 1882-1884, 1998.
209. Neef J, Gehrt A, Bulankina AV, Meyer AC, Riedel D, Gregg RG, Strenzke N, Moser T. The Ca2+ channel subunit beta2 regulates Ca2+ channel abundance and function in inner hair cells and is required for hearing. *J Neurosci* 29: 10730-10740, 2009.
210. Neyroud N, Tesson F, Denjoy I, Leibovici M, Donger C, Barhanin J, Faure S, Gary F, Coumel P, Petit C, Schwartz K, Guicheney P. A novel mutation in the potassium channel gene KVLQT1 causes the Jervell and Lange-Nielsen cardioauditory syndrome. *Nat Genet* 15: 186-189, 1997.
211. Nie L. KCNQ4 mutations associated with nonsyndromic progressive sensorineural hearing loss. *Curr Opin Otolaryngol Head Neck Surg* 16: 441-444, 2008.
212. Nin F, Hibino H, Doi K, Suzuki T, Hisa Y, Kurachi Y. The endocochlear potential depends on two K+ diffusion potentials and an electrical barrier in the stria vascularis of the inner ear. *Proc Natl Acad Sci U S A* 105: 1751-1756, 2008.
213. Nouvian R, Neef J, Bulankina AV, Reisinger E, Pangrsic T, Frank T, Sikorra S, Brose N, Binz T, Moser T. Exocytosis at the hair cell ribbon synapse apparently operates without neuronal SNARE proteins. *Nat Neurosci* 14: 411-413, 2011.
214. Nowotny M, Gummer AW. Nanomechanics of the subtectorial space caused by electromechanics of cochlear outer hair cells. *Proc Natl Acad Sci U S A* 103: 2120-2125, 2006.
215. Ohlemiller KK, Echteler SM. Functional correlates of characteristic frequency in single cochlear nerve fibers of the Mongolian gerbil. *J Comp Physiol A* 167: 329-338, 1990.
216. Ohmori H. Mechano-electrical transduction currents in isolated vestibular hair cells of the chick. *J Physiol* 359: 189-217, 1985.
217. Ohn TL, Rutherford MA, Jing Z, Jung S, Duque-Afonso CJ, Hoch G, Picher MM, Scharinger A, Strenzke N, Moser T. Hair cells use active zones with different voltage dependence of Ca2+ influx to decompose sounds into complementary neural codes. *Proc Natl Acad Sci U S A* 113: E4716-4725, 2016.
218. Oliver D, He DZ, Klocker N, Ludwig J, Schulte U, Waldegger S, Ruppersberg JP, Dallos P, Fakler B. Intracellular anions as the voltage sensor of prestin, the outer hair cell motor protein. *Science* 292: 2340-2343, 2001.
219. Oliver D, Taberner AM, Thurm H, Sausbier M, Arntz C, Ruth P, Fakler B, Liberman MC. The role of BKCa channels in electrical signal encoding in the mammalian auditory periphery. *J Neurosci* 26: 6181-6189, 2006.
220. Overstreet EH, III, Temchin AN, Ruggero MA. Basilar membrane vibrations near the round window of the gerbil cochlea. *J Assoc Res Otolaryngol* 3: 351-361, 2002.
221. Padmanarayana M, Hams N, Speight LC, Petersson EJ, Mehl RA, Johnson CP. Characterization of the lipid binding properties of Otoferlin reveals specific interactions between PI(4,5)P2 and the C2C and C2F domains. *Biochemistry* 53: 5023-5033, 2014.
222. Palmer AR, Russell IJ. Phase-locking in the cochlear nerve of the guinea-pig and its relation to the receptor potential of inner hair-cells. *Hear Res* 24: 1-15, 1986.
223. Pan B, Geleoc GS, Asai Y, Horwitz GC, Kurima K, Ishikawa K, Kawashima Y, Griffith AJ, Holt JR. TMC1 and TMC2 are components of the mechanotransduction channel in hair cells of the mammalian inner ear. *Neuron* 79: 504-515, 2013.
224. Pangrsic T, Gabrielaitis M, Michanski S, Schwaller B, Wolf F, Strenzke N, Moser T. EF-hand protein Ca2+ buffers regulate Ca2+ influx and

exocytosis in sensory hair cells. *Proc Natl Acad Sci U S A* 112: E1028-1037, 2015.
225. Pangrsic T, Lasarow L, Reuter K, Takago H, Schwander M, Riedel D, Frank T, Tarantino LM, Bailey JS, Strenzke N, Brose N, Muller U, Reisinger E, Moser T. Hearing requires otoferlin-dependent efficient replenishment of synaptic vesicles in hair cells. *Nat Neurosci* 13: 869-876, 2010.
226. Pangrsic T, Reisinger E, Moser T. Otoferlin: A multi-C2 domain protein essential for hearing. *Trends Neurosci* 35: 671-680, 2012.
227. Peng AW, Effertz T, Ricci AJ. Adaptation of mammalian auditory hair cell mechanotransduction is independent of calcium entry. *Neuron* 80: 960-972, 2013.
228. Peng AW, Gnanasambandam R, Sachs F, Ricci AJ. Adaptation independent modulation of auditory hair cell mechanotransduction channel open probability implicates a role for the lipid bilayer. *J Neurosci* 36: 2945-2956, 2016.
229. Peng AW, Salles FT, Pan B, Ricci AJ. Integrating the biophysical and molecular mechanisms of auditory hair cell mechanotransduction. *Nat Commun* 2: 523, 2011.
230. Pepermans E, Michel V, Goodyear R, Bonnet C, Abdi S, Dupont T, Gherbi S, Holder M, Makrelouf M, Hardelin JP, Marlin S, Zenati A, Richardson G, Avan P, Bahloul A, Petit C. The CD2 isoform of protocadherin-15 is an essential component of the tip-link complex in mature auditory hair cells. *EMBO Mol Med* 6: 984-992, 2014.
231. Petit C, Richardson GP. Linking genes underlying deafness to hair-bundle development and function. *Nat Neurosci* 12: 703-710, 2009.
232. Pickles JO, Comis SD, Osborne MP. Cross-links between stereocilia in the guinea pig organ of Corti, and their possible relation to sensory transduction. *Hear Res* 15: 103-112, 1984.
233. Platzer J, Engel J, Schrott-Fischer A, Stephan K, Bova S, Chen H, Zheng H, Striessnig J. Congenital deafness and sinoatrial node dysfunction in mice lacking class D L-type Ca2+ channels. *Cell* 102: 89-97, 2000.
234. Pollock LM, McDermott BM, Jr. The cuticular plate: A riddle, wrapped in a mystery, inside a hair cell. *Birth Defects Res C Embryo Today* 105: 126-139, 2015.
235. Pujol R L-RM, Lenoir M. Development of sensory and neural structures in the mammalian cochlea In: *Development of the Auditory System*, edited by Rubel EW PA, Fay RR. New York: Springer pp. 146-192, 1998.
236. Pyott SJ, Glowatzki E, Trimmer JS, Aldrich RW. Extrasynaptic localization of inactivating calcium-activated potassium channels in mouse inner hair cells. *J Neurosci* 24: 9469-9474, 2004.
237. Pyott SJ, Meredith AL, Fodor AA, Vazquez AE, Yamoah EN, Aldrich RW. Cochlear function in mice lacking the BK channel alpha, beta1, or beta4 subunits. *J Biol Chem* 282: 3312-3324, 2007.
238. Rabbitt RD, Clifford S, Breneman KD, Farrell B, Brownell WE. Power efficiency of outer hair cell somatic electromotility. *PLoS Comput Biol* 5: e1000444, 2009.
239. Rask-Andersen H, Erixon E, Kinnefors A, Lowenheim H, Schrott-Fischer A, Liu W. Anatomy of the human cochlea—implications for cochlear implantation. *Cochlear Implants Int* 12(Suppl 1): S8-S13, 2011.
240. Reichenbach T, Hudspeth AJ. A ratchet mechanism for amplification in low-frequency mammalian hearing. *Proc Natl Acad Sci U S A* 107: 4973-4978, 2010.
241. Ren T, He W, Kemp D. Reticular lamina and basilar membrane vibrations in living mouse cochleae. *Proc Natl Acad Sci U S A* 113: 9910-9915, 2016.
242. Rhode W, Cooper NP. Nonlinear mechanics in the apical turn of the chinchilla cochlea in vivo. *Auditory Neurosci* 3: 101-121, 1996.
243. Ricci AJ, Crawford AC, Fettiplace R. Active hair bundle motion linked to fast transducer adaptation in auditory hair cells. *J Neurosci* 20: 7131-7142, 2000.
244. Ricci AJ, Crawford AC, Fettiplace R. Tonotopic variation in the conductance of the hair cell mechanotransducer channel. *Neuron* 40: 983-990, 2003.
245. Ricci AJ, Fettiplace R. Calcium permeation of the turtle hair cell mechanotransducer channel and its relation to the composition of endolymph. *J Physiol* 506(Pt 1): 159-173, 1998.
246. Ricci AJ, Gray-Keller M, Fettiplace R. Tonotopic variations of calcium signalling in turtle auditory hair cells. *J Physiol* 524(Pt 2): 423-436, 2000.
247. Ricci AJ, Kennedy HJ, Crawford AC, Fettiplace R. The transduction channel filter in auditory hair cells. *J Neurosci* 25: 7831-7839, 2005.
248. Ricci AJ, Wu YC, Fettiplace R. The endogenous calcium buffer and the time course of transducer adaptation in auditory hair cells. *J Neurosci* 18: 8261-8277, 1998.
249. Richardson GP, de Monvel JB, Petit C. How the genetics of deafness illuminates auditory physiology. *Annu Rev Physiol* 73: 311-334, 2011.
250. Richardson GP, Lukashkin AN, Russell IJ. The tectorial membrane: One slice of a complex cochlear sandwich. *Curr Opin Otolaryngol Head Neck Surg* 16: 458-464, 2008.
251. Richter CP, Emadi G, Getnick G, Quesnel A, Dallos P. Tectorial membrane stiffness gradients. *Biophys J* 93: 2265-2276, 2007.
252. Roberts WM. Localization of calcium signals by a mobile calcium buffer in frog saccular hair cells. *J Neurosci* 14: 3246-3262, 1994.
253. Roberts WM, Jacobs RA, Hudspeth AJ. Colocalization of ion channels involved in frequency selectivity and synaptic transmission at presynaptic active zones of hair cells. *J Neurosci* 10: 3664-3684, 1990.
254. Robles L, Ruggero MA. Mechanics of the mammalian cochlea. *Physiol Rev* 81: 1305-1352, 2001.
255. Rose JE, Brugge JF, Anderson DJ, Hind JE. Phase-locked response to low-frequency tones in single auditory nerve fibers of the squirrel monkey. *J Neurophysiol* 30: 769-793, 1967.
256. Roth B, Bruns V. Postnatal development of the rat organ of Corti. II. Hair cell receptors and their supporting elements. *Anat Embryol (Berl)* 185: 571-581, 1992.
257. Roux I, Safieddine S, Nouvian R, Grati M, Simmler MC, Bahloul A, Perfettini I, Le Gall M, Rostaing P, Hamard G, Triller A, Avan P, Moser T, Petit C. Otoferlin, defective in a human deafness form, is essential for exocytosis at the auditory ribbon synapse. *Cell* 127: 277-289, 2006.
258. Ruel J, Emery S, Nouvian R, Bersot T, Amilhon B, Van Rybroek JM, Rebillard G, Lenoir M, Eybalin M, Delprat B, Sivakumaran TA, Giros B, El Mestikawy S, Moser T, Smith RJ, Lesperance MM, Puel JL. Impairment of SLC17A8 encoding vesicular glutamate transporter-3, VGLUT3, underlies nonsyndromic deafness DFNA25 and inner hair cell dysfunction in null mice. *Am J Hum Genet* 83: 278-292, 2008.
259. Ruggero MA, Rich NC. Furosemide alters organ of corti mechanics: Evidence for feedback of outer hair cells upon the basilar membrane. *J Neurosci* 11: 1057-1067, 1991.
260. Ruggero MA, Rich NC, Recio A, Narayan SS, Robles L. Basilar-membrane responses to tones at the base of the chinchilla cochlea. *J Acoust Soc Am* 101: 2151-2163, 1997.
261. Russell IJ, Drexl M, Foeller E, Vater M, Kossl M. Synchronization of a nonlinear oscillator: Processing the cf component of the echo-response signal in the cochlea of the mustached bat. *J Neurosci* 23: 9508-9518, 2003.
262. Russell IJ, Legan PK, Lukashkina VA, Lukashkin AN, Goodyear RJ, Richardson GP. Sharpened cochlear tuning in a mouse with a genetically modified tectorial membrane. *Nat Neurosci* 10: 215-223, 2007.
263. Safieddine S, El-Amraoui A, Petit C. The auditory hair cell ribbon synapse: From assembly to function. *Annu Rev Neurosci* 35: 509-528, 2012.
264. Safieddine S, Wenthold RJ. SNARE complex at the ribbon synapses of cochlear hair cells: Analysis of synaptic vesicle- and synaptic membrane-associated proteins. *Eur J Neurosci* 11: 803-812, 1999.
265. Salt AN, Inamura N, Thalmann R, Vora A. Calcium gradients in inner ear endolymph. *Am J Otolaryngol* 10: 371-375, 1989.
266. Salt AN, Melichar I, Thalmann R. Mechanisms of endocochlear potential generation by stria vascularis. *Laryngoscope* 97: 984-991, 1987.
267. Santos-Sacchi J, Song L, Zheng J, Nuttall AL. Control of mammalian cochlear amplification by chloride anions. *J Neurosci* 26: 3992-3998, 2006.
268. Schaechinger TJ, Oliver D. Nonmammalian orthologs of prestin (SLC26A5) are electrogenic divalent/chloride anion exchangers. *Proc Natl Acad Sci U S A* 104: 7693-7698, 2007.
269. Schmitz F, Konigstorfer A, Sudhof TC. RIBEYE, a component of synaptic ribbons: A protein's journey through evolution provides insight into synaptic ribbon function. *Neuron* 28: 857-872, 2000.
270. Schnee ME, Lawton DM, Furness DN, Benke TA, Ricci AJ. Auditory hair cell-afferent fiber synapses are specialized to operate at their best frequencies. *Neuron* 47: 243-254, 2005.
271. Schnee ME, Santos-Sacchi J, Castellano-Munoz M, Kong JH, Ricci AJ. Calcium-dependent synaptic vesicle trafficking underlies indefatigable release at the hair cell afferent fiber synapse. *Neuron* 70: 326-338, 2011.
272. Schneider ME, Dose AC, Salles FT, Chang W, Erickson FL, Burnside B, Kachar B. A new compartment at stereocilia tips defined by spatial and temporal patterns of myosin IIIa expression. *J Neurosci* 26: 10243-10252, 2006.
273. Seal RP, Akil O, Yi E, Weber CM, Grant L, Yoo J, Clause A, Kandler K, Noebels JL, Glowatzki E, Lustig LR, Edwards RH. Sensorineural deafness and seizures in mice lacking vesicular glutamate transporter 3. *Neuron* 57: 263-275, 2008.
274. Sellick PM, Patuzzi R, Johnstone BM. Measurement of basilar membrane motion in the guinea pig using the Mossbauer technique. *J Acoust Soc Am* 72: 131-141, 1982.
275. Sellick PM, Patuzzi R, Johnstone BM. Modulation of responses of spiral ganglion cells in the guinea pig cochlea by low frequency sound. *Hear Res* 7: 199-221, 1982.
276. Sewell WF. The effects of furosemide on the endocochlear potential and auditory-nerve fiber tuning curves in cats. *Hear Res* 14: 305-314, 1984.
277. Shera CA. Laser amplification with a twist: Traveling-wave propagation and gain functions from throughout the cochlea. *J Acoust Soc Am* 122: 2738-2758, 2007.

278. Spiden SL, Bortolozzi M, Di Leva F, de Angelis MH, Fuchs H, Lim D, Ortolano S, Ingham NJ, Brini M, Carafoli E, Mammano F, Steel KP. The novel mouse mutation Oblivion inactivates the PMCA2 pump and causes progressive hearing loss. *PLoS Genet* 4: e1000238, 2008.
279. Steel KP, Barkway C. Another role for melanocytes: Their importance for normal stria vascularis development in the mammalian inner ear. *Development* 107: 453-463, 1989.
280. Street VA, McKee-Johnson JW, Fonseca RC, Tempel BL, Noben-Trauth K. Mutations in a plasma membrane Ca2+-ATPase gene cause deafness in deafwaddler mice. *Nat Genet* 19: 390-394, 1998.
281. Strenzke N, Chakrabarti R, Al-Moyed H, Muller A, Hoch G, Pangrsic T, Yamanbaeva G, Lenz C, Pan KT, Auge E, Geiss-Friedlander R, Urlaub H, Brose N, Wichmann C, Reisinger E. Hair cell synaptic dysfunction, auditory fatigue and thermal sensitivity in otoferlin Ile515Thr mutants. *Embo j*, 2016.
282. Suchyna TM, Johnson JH, Hamer K, Leykam JF, Gage DA, Clemo HF, Baumgarten CM, Sachs F. Identification of a peptide toxin from Grammostola spatulata spider venom that blocks cation-selective stretch-activated channels. *J Gen Physiol* 115: 583-598, 2000.
283. Taberner AM, Liberman MC. Response properties of single auditory nerve fibers in the mouse. *J Neurophysiol* 93: 557-569, 2005.
284. Tan X, Beurg M, Hackney C, Mahendrasingam S, Fettiplace R. Electrical tuning and transduction in short hair cells of the chicken auditory papilla. *J Neurophysiol* 109: 2007-2020, 2013.
285. Temchin AN, Rich NC, Ruggero MA. Threshold tuning curves of chinchilla auditory-nerve fibers. I. Dependence on characteristic frequency and relation to the magnitudes of cochlear vibrations. *J Neurophysiol* 100: 2889-2898, 2008.
286. Temchin AN, Ruggero MA. Phase-locked responses to tones of chinchilla auditory nerve fibers: Implications for apical cochlear mechanics. *J Assoc Res Otolaryngol* 11: 297-318, 2010.
287. Teudt IU, Richter CP. Basilar membrane and tectorial membrane stiffness in the CBA/CaJ mouse. *J Assoc Res Otolaryngol* 15: 675-694, 2014.
288. Tritsch NX, Yi E, Gale JE, Glowatzki E, Bergles DE. The origin of spontaneous activity in the developing auditory system. *Nature* 450: 50-55, 2007.
289. Tucker T, Fettiplace R. Confocal imaging of calcium microdomains and calcium extrusion in turtle hair cells. *Neuron* 15: 1323-1335, 1995.
290. van der Heijden M, Versteegh CP. Energy flux in the cochlea: Evidence against power amplification of the traveling wave. *J Assoc Res Otolaryngol* 16: 581-597, 2015.
291. Verpy E, Leibovici M, Michalski N, Goodyear RJ, Houdon C, Weil D, Richardson GP, Petit C. Stereocilin connects outer hair cell stereocilia to one another and to the tectorial membrane. *J Comp Neurol* 519: 194-210, 2011.
292. Versteegh CP, Meenderink SW, van der Heijden M. Response characteristics in the apex of the gerbil cochlea studied through auditory nerve recordings. *J Assoc Res Otolaryngol* 12: 301-316, 2011.
293. Vogl C, Cooper BH, Neef J, Wojcik SM, Reim K, Reisinger E, Brose N, Rhee JS, Moser T, Wichmann C. Unconventional molecular regulation of synaptic vesicle replenishment in cochlear inner hair cells. *J Cell Sci* 128: 638-644, 2015.
294. Vollrath MA, Eatock RA. Time course and extent of mechanotransducer adaptation in mouse utricular hair cells: Comparison with frog saccular hair cells. *J Neurophysiol* 90: 2676-2689, 2003.
295. Vu AA, Nadaraja GS, Huth ME, Luk L, Kim J, Chai R, Ricci AJ, Cheng AG. Integrity and regeneration of mechanotransduction machinery regulate aminoglycoside entry and sensory cell death. *PLoS One* 8: e54794, 2013.
296. Wang HC, Bergles DE. Spontaneous activity in the developing auditory system. *Cell Tissue Res* 361: 65-75, 2015.
297. Wangemann P. Supporting sensory transduction: Cochlear fluid homeostasis and the endocochlear potential. *J Physiol* 576: 11-21, 2006.
298. Wangemann P. The role of pendrin in the development of the murine inner ear. *Cell Physiol Biochem* 28: 527-534, 2011.
299. Wangemann P, Itza EM, Albrecht B, Wu T, Jabba SV, Maganti RJ, Lee JH, Everett LA, Wall SM, Royaux IE, Green ED, Marcus DC. Loss of KCNJ10 protein expression abolishes endocochlear potential and causes deafness in Pendred syndrome mouse model. *BMC Med* 2: 30, 2004.
300. Wangemann P, Liu J, Marcus DC. Ion transport mechanisms responsible for K+ secretion and the transepithelial voltage across marginal cells of stria vascularis in vitro. *Hear Res* 84: 19-29, 1995.
301. Wangemann P, Nakaya K, Wu T, Maganti RJ, Itza EM, Sanneman JD, Harbidge DG, Billings S, Marcus DC. Loss of cochlear HCO3- secretion causes deafness via endolymphatic acidification and inhibition of Ca2+ reabsorption in a Pendred syndrome mouse model. *Am J Physiol Renal Physiol* 292: F1345-1353, 2007.
302. Webb SW, Grillet N, Andrade LR, Xiong W, Swarthout L, Della Santina CC, Kachar B, Muller U. Regulation of PCDH15 function in mechanosensory hair cells by alternative splicing of the cytoplasmic domain. *Development* 138: 1607-1617, 2011.
303. Wersinger E, McLean WJ, Fuchs PA, Pyott SJ. BK channels mediate cholinergic inhibition of high frequency cochlear hair cells. *PLoS One* 5: e13836, 2010.
304. Wiederhold ML. Variations in the effects of electric stimulation of the crossed olivocochlear bundle on cat single auditory-nerve-fiber responses to tone bursts. *J Acoust Soc Am* 48: 966-977, 1970.
305. Willemin JF, Dandliker R, Khanna SM. Heterodyne interferometer for submicroscopic vibration measurements in the inner ear. *J Acoust Soc Am* 83: 787-795, 1988.
306. Wingard JC, Zhao HB. Cellular and deafness mechanisms underlying connexin mutation-induced hearing loss—a common hereditary deafness. *Front Cell Neurosci* 9: 202, 2015.
307. Wong AB, Rutherford MA, Gabrielaitis M, Pangrsic T, Gottfert F, Frank T, Michanski S, Hell S, Wolf F, Wichmann C, Moser T. Developmental refinement of hair cell synapses tightens the coupling of Ca2+ influx to exocytosis. *Embo j* 33: 247-264, 2014.
308. Wood JD, Muchinsky SJ, Filoteo AG, Penniston JT, Tempel BL. Low endolymph calcium concentrations in deafwaddler2J mice suggest that PMCA2 contributes to endolymph calcium maintenance. *J Assoc Res Otolaryngol* 5: 99-110, 2004.
309. Wu DK, Kelley MW. Molecular mechanisms of inner ear development. *Cold Spring Harb Perspect Biol* 4: a008409, 2012.
310. Wu YC, Art JJ, Goodman MB, Fettiplace R. A kinetic description of the calcium-activated potassium channel and its application to electrical tuning of hair cells. *Prog Biophys Mol Biol* 63: 131-158, 1995.
311. Wu YC, Ricci AJ, Fettiplace R. Two components of transducer adaptation in auditory hair cells. *J Neurophysiol* 82: 2171-2181, 1999.
312. Xiong W, Grillet N, Elledge HM, Wagner TF, Zhao B, Johnson KR, Kazmierczak P, Muller U. TMHS is an integral component of the mechanotransduction machinery of cochlear hair cells. *Cell* 151: 1283-1295, 2012.
313. Yamoah EN, Lumpkin EA, Dumont RA, Smith PJ, Hudspeth AJ, Gillespie PG. Plasma membrane Ca2+-ATPase extrudes Ca2+ from hair cell stereocilia. *J Neurosci* 18: 610-624, 1998.
314. Yan Z, Zhang W, He Y, Gorczyca D, Xiang Y, Cheng LE, Meltzer S, Jan LY, Jan YN. Drosophila NOMPC is a mechanotransduction channel subunit for gentle-touch sensation. *Nature* 493: 221-225, 2013.
315. Yasunaga S, Grati M, Cohen-Salmon M, El-Amraoui A, Mustapha M, Salem N, El-Zir E, Loiselet J, Petit C. A mutation in OTOF, encoding otoferlin, a FER-1-like protein, causes DFNB9, a nonsyndromic form of deafness. *Nat Genet* 21: 363-369, 1999.
316. Yoon YJ, Steele CR, Puria S. Feed-forward and feed-backward amplification model from cochlear cytoarchitecture: An interspecies comparison. *Biophys J* 100: 1-10, 2011.
317. Zhang L, Gualberto DG, Guo X, Correa P, Jee C, Garcia LR. TMC-1 attenuates C. elegans development and sexual behavior in a chemically defined food environment. *Nature Comm* 6: 6345, 2015.
318. Zhao B, Muller U. The elusive mechanotransduction machinery of hair cells. *Curr Opin Neurobiol* 34: 172-179, 2015.
319. Zhao B, Wu Z, Grillet N, Yan L, Xiong W, Harkins-Perry S, Muller U. TMIE is an essential component of the mechanotransduction machinery of cochlear hair cells. *Neuron* 84: 954-967, 2014.
320. Zheng J, Shen W, He DZ, Long KB, Madison LD, Dallos P. Prestin is the motor protein of cochlear outer hair cells. *Nature* 405: 149-155, 2000.
321. Zheng L, Sekerkova G, Vranich K, Tilney LG, Mugnaini E, Bartles JR. The deaf jerker mouse has a mutation in the gene encoding the espin actin-bundling proteins of hair cell stereocilia and lacks espins. *Cell* 102: 377-385, 2000.
322. Zidanic M, Brownell WE. Fine structure of the intracochlear potential field. I. The silent current. *Biophys J* 57: 1253-1268, 1990.
323. Zwislocki JJ, Kletsky EJ. Tectorial membrane: A possible effect on frequency analysis in the cochlea. *Science* 204: 639-641, 1979.